Untargeted metabolomics reveals anion and organ-specific biochemistry of salinity tolerance in willow

Eszter Sas[1], Adrien Frémont[1], Emmanuel Gonzalez[2,3], Mathieu Sarrazin[4], Simon Barnabé[5], Michel Labrecque[1,6], Nicholas James Beresford Brereton[7†] and Frédéric Emmanuel Pitre[1,6]

[1] Institut de recherche en biologie végétale (IRBV), Département de sciences biologiques, Université de Montréal - 4101 Sherbrooke East, Montreal, QC H1X 2B2, Canada
[2] Canadian Centre for Computational Genomics (C3G) - Department of Human Genetics, McGill University, 740 Dr. Penfield avenue, Montreal, QC H3A 0G1, Canada.
[3] Microbiome Research Platform - McGill Interdisciplinary Initiative in Infection and Immunity (MI4), Genome Centre, McGill University, Montreal, QC, Canada
[4] Centre d'Étude des Procédés Chimiques du Québec (CÉPROCQ), Collège de Maisonneuve, 6220 Rue Sherbrooke East, Montréal, QC H1N 1C1, Canada
[5] Département de chimie, biochimie et physique, Université du Québec à Trois- Rivières, 3351 boulevard des Forges, Trois-Rivières, QC G8Z 4M3, Canada
[6] Montreal Botanical Garden, 4101 Sherbrooke East, Montreal, QC H1X 2B2, Canada
[7] UCD School of Biology and Environmental Science, University College Dublin, Belfield, Dublin 4, Ireland

† Corresponding author: nicholas.brereton@ucd.ie

Key words: Salt stress • Metabolomics • *Salix* • Sulfate / Sulfur • Sulphate / Sulphur • Chloride • Anion

1 Abstract

Willows can alleviate soil salinisation while generating sustainable feedstock for biorefinery, yet the metabolomic adaptations underlying their salt tolerance remain poorly understood. Testing two environmentally abundant salts, the response of *Salix miyabeana* was assessed after treatment with a moderate concentration of NaCl, and both moderate and high concentrations of Na_2SO_4 in a 12-week pot trial. Willows tolerated salts across all treatments (up to 9.1dS m^{-1} soil EC_e), maintaining photosynthesis and biomass while selectively partitioning ions, confining Na^+ to roots and accumulating Cl^- and SO_4^{2-} in the canopy, and adapting to osmotic stress via reduced stomatal conductance. Untargeted LC-MS/MS captured over 5,000 putative compounds, characterising the baseline willow metabolome, including 278 core compounds constitutively produced across organs. Comparative statistical analyses revealed widespread metabolic reprogramming in response to soil salinity, altering 28% of the overall metabolome, and highlighting organ-tailored regulation. Comparing both salt forms at equimolar sodium, generalised salinity responses were limited to 3% of the metabolome, predominantly in roots. Anion-specific metabolomic responses were more extensive, with NaCl reducing carbohydrates and TCA intermediates, thereby exerting pressure on carbon and energy resources, alongside the accumulation of root structuring compounds, antioxidants flavonoids, and fatty acids. In contrast, Na_2SO_4 salinity triggered accumulation of sulphur-containing larger peptides, suggesting that excess sulphate incorporation leverage ion toxicity to produce specialized salt-tolerance associated metabolites. This high-depth picture of the willow metabolome underscores the importance of capturing plant adaptations to salt stress at organ-scale and considering ion-specific contributions to soil salinity.

2 Introduction

Soil salinisation represents a major threat to agricultural productivity and environmental health on a global scale. It is estimated that over 20% of irrigated cropland is impacted by salt accumulation (FAO, 2015), reducing yields and critical ecosystem biodiversity (Zörb et al., 2019). Climate change and human activities are predicted to intensify both natural and anthropogenic soil salinisation processes, further threatening food security (Singh, 2021). While salt stress research typically investigates NaCl, Na_2SO_4, derived from anthropogenic sources like industrial sulphur emissions and agricultural practices, as well as natural volcanic and marine environments (Dick et al., 2008), represents another widespread salt. The use of salt-tolerant biomass crops able to sequester salt and improve soil health, could help reclaim and repurpose salt-impacted areas (Abreu et al., 2022; Quinn et al., 2015).

Soil salinisation results from soluble ions accumulation such as Na^+, K^+, Mg^{2+}, Ca^{2+}, Cl^-, SO_4^{2-} and CO_3^{2-}. When in contact with roots, these ions can induce both osmotic stress and ion toxicity (Munns and Tester, 2008). The osmotic component, primarily driven by any dissolved salt concentration, alters water potential gradients, disrupting cell turgor pressure and elongation. In response, stomatal closure limits water loss via transpiration but also impairs photosynthate supply, ultimately constraining growth through both water deficit and reduced carbon availability (Munns et al., 2020b). Ion toxicity, however, is dependent on the nature of the ion, with different elements inducing unique patterns of signalling, transport, oxidative damage, energy allocation, and hormone-regulated growth processes (Llanes et al., 2013; Reginato et al., 2021; Richter et al., 2019).

Chloride (Cl^-), an essential micronutrient for plants, contributes to vital physiological processes (Wege et al., 2017). As a major osmotically active solute, chloride fluxes are involved in vacuolar turgor required for cell expansion and are implicated in stomatal aperture regulation, contributing to water balance and gas exchange (Teakle and Tyerman, 2010). Additionally, chloride acts as a counter-ion, regulating membrane potential, intracellular pH gradients, electrical signalling in the cytoplasm (White and Broadley, 2001) and serves as a cofactor in the oxygen-evolving complex of photosystem II (Ifuku, 2015). However, in salt-impacted soils, excess chloride damages plants, leading to impaired photosynthesis, reduced NO_3^- uptake (Abdelgadir et al., 2005) and general enzymatic activity (Geilfus, 2018). In contrast, sulphate (SO_4^{2-}), the major bioavailable form of sulphur, is an essential macronutrient involved in physiological and biochemical processes (Prasad and Shivay, 2018; Watanabe and Hoefgen, 2019). Sulphur is required for the production of the amino acids cysteine and methionine, peptide derivatives such as glutathione, and disulphide bonds contributing to enzyme activity and stability. The production of chlorophyll, vitamins and certain plant defence specialised metabolites, such as glucosinolates, also depend upon sulphur (Chan et al., 2019; Rausch and Wachter, 2005). Plants regulate sulphate uptake and assimilation through sulphate specific transporters to avoid toxicity (Buchner et al., 2004), however in some crop species, such as *Brassica rapa*, excess sulphate ions can create nutrient deficiency by competing with the absorption of other ions, especially calcium and phosphorus (Reich et al., 2017).

Plants mediate salt stress through a coordinated series of physiological, structural, biochemical and molecular adjustments (Arif et al., 2020; Deinlein et al., 2014; Gupta and Huang, 2014; van Zelm et al., 2020; Yang and Guo, 2018). Although pathways vary between plant species (Sanchez et al., 2008) and depend on the type of ions involved (Reich et al., 2017; Richter et al., 2019), key tolerance mechanisms include osmotic regulation, ion homeostasis, antioxidant defence, and growth modulation. A primary adaptive response to osmotic stress is the accumulation of osmolytes, which regulate water status by reducing cell osmotic potential (D'Amelia et al., 2018). This common osmotic stress response is not exclusively induced by excess salt nor is dependent on salt type (Munns, 2002). Osmolytes include inorganic ions (Rodriguez et al., 1997; Wege et al., 2017) and organic compounds such as amino acids (e.g. proline), polyamines (e.g. spermidine), quaternary ammonium compounds (e.g. glycine betaine), sugars (e.g. sucrose, trehalose), and polyols (e.g. mannitol, sorbitol) (D'Amelia et al., 2018; Slama et al., 2015; Yang and Guo, 2018). While the biosynthesis of these osmoprotectants imposes a metabolic energy cost (Munns et al., 2020a), their functions extend beyond osmotic adjustment to detoxification processes such as antioxidant activity and chaperone-mediated protein stabilisation (Yancey, 2005). The upregulation of enzymatic (e.g. superoxide dismutase SOD, catalase CAT, peroxidase POX) and non-enzymatic (e.g. glutathione, ascorbate, flavonoids, anthocyanins) antioxidants is crucial for mitigating damage to cellular components such as lipids, proteins, and DNA caused by reactive oxygen species (ROS) (Gill and Tuteja, 2010a). More generally, plants avoid cytotoxicity and maintain ion homoeostasis through salt exclusion from roots, compartmentalisation into the vacuole or apoplast, selective transport and excretion through salt glands. Additionally, hormonal signalling (Ryu and Cho, 2015), modification of root architecture (Zou et al., 2022), xylem alteration and loading (Janz et al., 2012) and symbiotic associations with microorganisms such as arbuscular mycorrhizal fungi (Evelin et al., 2009) also play significant roles in enhancing plant tolerance to salinity.

Salicaceae, including poplars (*Populus sp.)* and willows (*Salix sp.*), are common phytoremediation and biorefinery crops on marginal lands (Brereton et al., 2017; Dimitriou and Aronsson, 2005; Gonzalez et al., 2018; Rodzkin and Volk, 2018; Sas et al., 2021; Volk et al., 2006), with high potential for growth on salinised soils. Some cultivars can maintain transpiration and growth under saline conditions up to 6-8 dS m^{-1} (Bilek et al., 2020; Chen and Polle, 2010; Huang et al., 2020; Mirck and Zalesny, 2015). This tolerance likely engages high metabolic diversity, including reactive oxygen species (ROS) protective phenolics and other antioxidants (Sui

and Wang, 2020; Zhou et al., 2020). However, understanding of the metabolomic toolkit employed beyond these compounds, and their variation across different organs and salts, remains limited.

In this study, the shared and unique metabolomic adjustments to moderate NaCl, moderate Na_2SO_4 and high Na_2SO_4 salinity treatment are assessed across multiple organs (Fig.1) to determine generalised and ion-specific salt tolerance metabolome in willow.

3 Methods

3.1 Experimental design, plant growth, sample collection and physiological traits

The willow cultivar *Salix miyabeana* 'SX64' was grown from cuttings in a polyethylene grow tunnel within 15 L pots filled with all-purpose growing soil (Promix™), sand and vermiculite (1:1:1 volume-based). After 56 days of growth for root establishment, salt treatments were applied every 3 days during watering over 28 days to progressively build up soil salinity and to avoid salt shock response (Shavrukov, 2013). The four treatments were: tap water control (EC_{water}=0.3 mS cm^{-1}), 51mM NaCl ($EC_{solution}$=6.5 dS m^{-1}) and 26mM Na_2SO_4 ($EC_{solution}$=6.7 dS m^{-1}), both considered moderately saline, and 51mM Na_2SO_4 ($EC_{solution}$=13.4 dS m^{-1}), considered highly saline (Mirck and Zalesny, 2015). The treatments were arranged in a randomised block design with seven replicate plants (seven independent pots, n=7) per treatment (Fig.1). Leaves, stems, and roots were sampled after 28 days of treatment (84 days of growth). A representative subsample of each fraction was immediately flash-frozen in liquid nitrogen and stored at -70°C for metabolomic analysis.

Shoot heights and numbers were measured weekly. Fresh weight (FW) at harvest, oven-dried biomass weight (DW) and moisture content were measured for each organ. The LICOR-600 porometer/fluorometer was used to measure photosynthetic parameters, including stomatal conductance and the quantum efficiency in light of photosystem II ΦPSII (Genty et al., 1989). Soil salinity was inferred at harvest from electroconductivity of the supernatant solution from a soil:water mixture (1:1) and converted to the electroconductivity of saturated soil extract (EC_e) using the correlation EC_e=2.23 $EC_{(1:1)}$-0.58 (R^2=0.98) (Sonmez et al., 2008).

Elemental analysis of roots, stems, and leaves was performed on ground dry biomass (<500 µm) by Natural Resources Analytical Laboratory at University of Alberta (AB, Canada). Briefly, 0.1±0.02 g of sample was digested overnight, with 5 mL of Trace Metal Grade HNO_3 using the Microwave Accelerated Reaction System (method EPA 3051a (modified)), diluted to 25 mL with milliQ water and analysed for mineral nutrients (Al, B, Ca, Cu, Fe, K, Mg, Mn, Mo, Na, Ni, P, S, Zn) using a Thermo iCAP6300 Duo inductively coupled plasma-optical emission spectrometer (ICP-OES). The anions Cl^- and SO_4^{2-} were determined by extracting 0.2±0.01 g of dry sample with 50 mL of 2% acetic acid using a reciprocal shaker for 30 min, followed by a 0.45 µm PTFE syringe filtration. Chloride and sulphate were measured using the ferrithiocyante colorimetric method (EPA Method 325.2) and the barium chloride turbidimetric method (EPA Method 375.4), respectively.

3.2 Extraction of metabolites

Metabolites from willow roots, stems and leaves were extracted according to De Vos et al. (2007) with some modifications. Briefly, plant tissues were freeze-dried for 72 hours and homogenised using a precooled bead mill Tissuelyser II (Qiagen) at 30 Hz, for 2-4 cycles of 60 seconds each. From the dry tissue powder, 50±0.5 mg was suspended in 1 mL of methanol:water (75:25%v/v), also containing the internal quantitative standard resorcinol at 5 mmol L^{-1}. Samples were vortexed for 10 s, sonicated in a 135 W/42 Hz ultrasound bath for 10 min at room temperature and centrifuged at 11,000xg for 2 min at 20°C. The supernatant was filtered through a 0.2 µm centrifuge filter, diluted by 4 with methanol 75% and placed in the LC-MS/MS autosampler conditioned at 4°C.

3.3 Liquid chromatography-tandem mass spectrometry (LC-MS/MS) acquisition

Chromatographic separation was performed using an Agilent 1260 Infinity system, where 10 µL of extract was injected onto a Zorbax Eclipse Plus C18 column (4.6 × 100 mm, 3.5 µm) at 30 °C. Mobile phase was solvent A (water, 5% methanol, 0.1% formic acid) and solvent B (methanol, 0.1% formic acid) with a flow rate of 0.4 mL min^{-1} and an 80-minute elution gradient: 100% A hold for 20 min, then a linear increase from 0% to 100% B over 50 min and 100% B hold for 10 min. This gradient allowed detection of highly water-soluble (polar) compounds within the first isocratic phase. Untargeted full-scan (100–1,300 Da) MS acquisition was performed on extracts from all three organs (roots, stems and leaves) of each of the seven replicates (84 samples total),

151 blanks and quality control samples using an Agilent Q-TOF 6530B mass spectrometer equipped with an Agilent
152 Jet Stream ion source operating in positive ion mode (ESI (+)). Gas temperature was 300 °C, drying gas flow was
153 5 L min^{-1}, and the nebuliser pressure was 45 psig. Sheath gas temperature was 250 °C with a gas flow of 11 L
154 min^{-1}. Data-dependent MS/MS acquisition was performed on three biological organ replicates per treatment
155 and acquired at collision energy of 20 and 35 eV. Precursor isolation used an intensity threshold set to 500,
156 with a maximum of 4 precursors per cycle and 3 spectra per precursor released after 0.3 min.

157 ***3.4 Untargeted metabolite data processing***

158 Raw LC-MS data were converted to mzML files by using msConvert (Chambers et al., 2012) and processed using
159 MZmine 3.3.0 (Schmid et al., 2023) (Fig.1). Background noise cut-off was 1,000 for MS spectra and 0 for MS/MS
160 spectra, with a minimum 5,000 peak intensity threshold for feature detection. Chromatogram deconvolution
161 used the local minimum search algorithm, isotopes were grouped and features alignment across samples was
162 performed with 20 ppm mass tolerance (80% weighting) and 1 min retention time tolerance (20% weighting).
163 Feature quality control filtering applied isotope patterns (minimum two), minimal occurrence of four across all
164 samples, and a maximal blank:sample average ratio (1:3). Features eluting within <0.2 min retention time and
165 with peak shape correlated by >85% (MZmine metaCorrelate algorithm) were assigned to a feature correlation
166 group and used for curation of adducts, complex formation, and in source fragments.

167 ***3.5 Metabolites annotation and molecular networking***

168 The feature annotation pipeline used unsupervised and supervised searches across multiple databases
169 integrated with cheminformatic tools (Fig.1). An initial unsupervised annotation step used *in silico* prediction
170 with SIRIUS, combining raw formula and structural elucidation CSI:FingerID (Dührkop et al., 2019), as well as
171 compound class annotation with CANOPUS (Dührkop et al., 2021). In parallel, all features were searched
172 against a set of MS and MS/MS databases, including general databases available in the GNPS environment
173 (including GNPS, MassBank and ReSpect) as well as experiment- and organism-specific databases (PlantCyc
174 (Hawkins et al., 2021), CEU mass mediator (Gil-de-la-Fuente et al., 2019), an in-house library for Salicaceae
175 based on literature as well as authentic standards). Annotation candidate information was standardised for
176 comparison across tools, and the best hit for each feature selected after quality assessment and prioritisation
177 based on integrated confidence/accuracy scores, MS/MS alignment scores, and MS match precision (minimal
178 difference between experimental and predicted compound mass, adduct prediction) to generate a list of
179 putative compounds from combined tools outputs.

180 In a second supervised step, annotation of significantly differentially abundant compounds was refined using
181 data-driven and knowledge-based curation. Data-driven curation uses feature-based ion identity molecular
182 networking (Z. Zhou et al., 2022) based on cosine and/or Spec2Vec metrics (Huber et al., 2021) of spectral
183 similarity within subnetworks, and manual resolution of ambiguities. Knowledge-driven curation takes
184 advantage of published compound lists and spectra from comparable experiments and plant species not
185 deposited in public databases to improve annotation.

186 Each putative compound annotation is assigned a confidence level (1-4) (Schymanski et al., 2014; Sumner et
187 al., 2007) and is reported in supporting information – Table S4, following best reporting practices (Alseekh et
188 al., 2021). Chemical taxonomy was assigned to metabolites using the Natural Product Classification system
189 (Kim et al., 2021). Molecular networks were generated in the GNPS analysis environment (Nothias et al., 2020)
190 and visualisation used cosine metrics (at 0.6 threshold) within Cytoscape software (Shannon et al., 2003).

191 ***3.6 Statistical analysis***

192 Physiological and metabolomic data were processed using R (R Core Team, 2022) and statistical significance
193 was set at a Benjamin-Hochberg (BH) false discovery rate (FDR) adjusted p-value threshold of <0.05.
194 Physiological comparisons between treatments used a two-way ANOVA, followed by a Tukey HSD *post hoc* test
195 (n=7, except n = 3 for mineral element analysis). Metabolite peak areas were log-transformed and normalised
196 using EigenMS (Karpievitch et al., 2014) prior to statistical analysis (Fig.1). To identify differentially abundant
197 (DA) metabolites, pairwise comparisons of peak area for each treatment (n=7) were performed against controls
198 using either a t-test or Wilcoxon rank sum test with FDR (BH) control, depending on whether assumptions of
199 normality and equal variance were met, or through detection as structural zeros (He et al., 2014) (metabolites
200 detected ≥4 replicates of one condition, and not detected in any replicates of the compared condition). For
201 metabolite comparison across organs, a Kruskal-Wallis test was first performed before *post hoc* pairwise

comparisons between each organ pair (Wilcoxon rank sum tests with FDR control). The core metabolome was tentatively defined as compounds that did not significantly vary across control organs and meet a metabolic stability coefficient of variation of peak area below 30%. Principal component analysis (PCA) was performed using MixOmics package (Rohart et al., 2017) and PERMANOVA on Bray-Curtis distances was used to test significant differences between groups.

4 Results

4.1 Physiological effects of salt treatments and mineral elements accumulation

After 28 days of salinity treatments, soil electrical conductivity (EC_e) was 0.9±0.2 dS m^{-1} in controls (Fig.2a) and was significantly higher in both moderate NaCl and Na_2SO_4 treatments, at 6.5±0.2 and 5.5±0.5 dS m^{-1} (Tukey HSD, $\alpha<0.05$). High Na_2SO_4 significantly increased soil conductivity further to 9.1±0.5 dS m^{-1}.

Willows maintained a healthy phenotype throughout the experiment (Fig.2b) and salt treatments did not induce significant differences in aboveground growth rates or organ biomass yields compared to controls (Supporting information Fig.S1-S3), with total biomass averaging 131±5 g dry matter (DM) (Fig.2c). Quantum efficiency ΦPSII ranged from 0.44-0.61 and was not significantly different between treatments (Fig.2d). Salt-treated willows showed significant reductions in stomatal conductance to water vapor (g_{sw}) ranging from 0.13-0.19 mol m^{-2} s^{-1} (Fig.2e), compared to g_{sw} of 0.29±0.04 mol m^{-2} s^{-1} in control willows. Leaf moisture content (MC) was 1.97±0.07 g_{H2O} g_{DM}^{-1} in controls and significantly increased to 2.28±0.10 g_{H2O} g_{DM}^{-1} under moderate NaCl treatment. Moderate Na_2SO_4 resulted in intermediate leaf MC, at 2.09±0.04 g_{H2O} g_{DM}^{-1}, while high Na_2SO_4 treatment significantly decreased compared to both moderate salt treatments, measuring 1.75±0.04 g_{H2O} g_{DM}^{-1} (Fig.2f). None of the treatments induced significant differences in stem moisture content, which was maintained at an average of 1.34±0.03 g_{H2O} g_{DM}^{-1}.

Total sodium content was 2.78±0.1 mmol(Na) in controls, 9.4±0.3 mmol(Na) in moderate NaCl, 10.1±0.1 in moderate Na_2SO_4 and 13.0±0.1 mmol(Na) in high Na_2SO_4-treated willows (Fig.3a). Comparison at the organ scale (Fig.3b) revealed the highest sodium concentration in roots, 3-fold higher than controls in all salt treatments. Total chloride content was significantly higher in NaCl treatment, with 26.3±2.1 mmol(Cl) as compared to an average of 6.8±0.2 mmol(Cl) for controls and Na_2SO_4 treatments. In NaCl treatment, leaves had the highest concentration of Cl at 575.4±26.5 µmol(Cl) g_{DW}^{-1}, representing a 3.4-fold increase compared to controls; while accumulation in stems and roots was below 190 µmol(Cl) g_{DW}^{-1}, but still 4.3 to 5.5-fold higher than controls. Total sulphur content was significantly higher in trees of both Na_2SO_4 treatments, at similar 14.1±0.5 and 15.7±1.9 mmol(S), as compared to 7.4±0.4 mmol(S) in controls and 8.5±0.2 mmol(S) in NaCl. Sulphur concentration significantly increased from 84.3±6.1 µmol(S) g_{DW}^{-1} in control roots to 147.9±6.1 µmol(S) g_{DW}^{-1} in Na_2SO_4-treated roots and from 161.0±11.1 µmol(S) g_{DW}^{-1} to 229.1±7.5 µmol(S) g_{DW}^{-1} in leaves. At the whole plant scale, the proportion of inorganic sulphur did not vary significantly across treatments, averaging 27% of the total sulphur present as inorganic SO_4^{2-} (Supporting information – Fig.S5). Total potassium content was 21.3±0.6 mmol(K) in controls and significantly higher in both moderate and high Na_2SO_4 treatments, with similar content of 28.9±0.2 and 28.4±2.3 mmol(K) respectively. Potassium concentration tended to decrease in salt-treated roots but increased in salt-treated leaves compared to controls. Across all four treatments, there were no significant variations in total phosphorus, calcium and magnesium content (Fig.3a). However, calcium concentration in leaves significantly decreased in both Na_2SO_4-treated plants compared to controls while leaf magnesium concentration significantly increased in NaCl-treated plants only, compared to controls (Fig.3b).

4.2 Organ partitioning of the Salix metabolome

After 84 days of growth, untargeted metabolomic profiling of control willows, without salt treatment, revealed a total of 5,043 metabolic compounds across all three organs, with 2,063 compounds in roots, 2,950 compounds in stems, and 3,601 compounds in leaves (Fig.4a). Shannon and inverse Simpson indices showed a significant sequential increase in metabolic diversity from roots to stems to leaves (Fig.4b). Principal Component Analysis (PCA) separated samples based on organ (Fig.4c), PC1 and PC2 explaining 52% and 26% of variance, respectively, with significant differences between groups (*PERMANOVA*, p-value < 0.05). Leaves and stems exclusively shared 481 compounds, stems and roots exclusively shared 371 compounds while leaves and roots exclusively shared 83 compounds (Fig.4d).

A total of 1318 compounds were present in all three organs (Fig.4d), representing 73-96% of cumulative peak area in each organ (Fig.4e). Differential abundance analysis between organs showed that, of these shared compounds, 278 did not significantly differ. They were defined as "core metabolites" and included 29 flavonoids, 14 phenolic acids, 12 phenylpropanoids, 22 small peptides, 11 tryptophan alkaloids, 9 pseudoalkaloids, 10 nucleosides, 8 saccharides, 8 monoterpenoids and 4 fatty acids and conjugates (Fig.4f). High-intensity compounds included adenosine, glutamate, 12-tetradecenoic acid, myrciacitrin III, apigenin 7-O-neohesperidoside, kaempferol 3-O-glucoside (astragalin), salicortin, salicin, benzaldehyde, 4-o-caffeoylshikimic acid, secoxyloganin, 7-O-p-coumaroyl loganin, nicotinamide, galactosylglycerol and fructose (Supporting information - Tables S3,S4).

Conversely, 3,259 compounds were organ-specialised metabolites with significantly increased abundance in one organ, including 1,719 compounds exclusively detected in leaves, 780 in stems and 291 in roots. Leaf-specialised compounds were dominated by the terpenoid pathway (Fig.4g), with a high number of (seco)iridoid monoterpenoids, diterpenoids, steroids, (apo)carotenoids, as well as the alkaloids pathway, particularly tyrosine and tryptophan derived alkaloids. Stem-specialised compounds were dominated by phenylpropanoids, lignans and fatty esters whereas root-specialised compounds were dominated by saccharides and amino acids glycosides. Each organ also had a highly specific set of flavonoids and small peptides. Interestingly, 19% of root-specialised compounds were highly water soluble (polar), compared to 5% of stem-specialised and 10% of leaf-specialised compounds (Supporting information – Fig.S6).

4.3 Salix metabolomic response to moderate and high Na_2SO_4

Principle component analysis (PCA) separated samples by control, moderate and high Na_2SO_4 treatments in roots *(PERMANOVA*, p-value <0.05), with PC1 explaining 17% and PC2 explaining 11% of the variance, while no separation was observed between treatments in stems and leaves (Fig.5a). Moderate Na_2SO_4 led to 571 differentially abundant (DA) compounds across the whole plant, including 218 in roots, 105 in stems and 248 in leaves (Fig.5b,d). Comparatively, high Na_2SO_4 led to 976 DA compounds across the whole plant, including 574 in roots, 131 in stems and 271 in leaves (Fig.5c,d).

Taken together, the Na_2SO_4-salt response involved 989 DA compounds distributed across the main pathways as 260 shikimates/phenylpropanoids, 133 alkaloids, 84 carbohydrates, 79 amino acids/peptides, 73 terpenoids, 51 fatty acids and 25 polyketides (Fig.5e). In response to moderate Na_2SO_4 treatment, DA compounds in roots and stems were mostly depleted (58-60%), while DA compounds in leaves were mostly enriched (85%) (Fig.5d,h). Higher Na_2SO_4 induced a larger metabolite enrichment across most pathways, except for further depletion in carbohydrates, while stems maintained a reduced metabolite pattern and leaves maintained increased metabolites across the major pathways.

Over the whole plant, 327 compounds were consistently altered in both moderate and high Na_2SO_4 treatments, representing 21% of DA compounds in roots, 24% in stems and 53% in leaves (Fig.5f). This consistent response was further reflected in a R^2=0.93 correlation between the fold changes (log_2) moderate and high Na_2SO_4 treatments compared to controls (Fig.5g).

In roots, moderate Na_2SO_4 reduced 45 compounds within shikimates/phenylpropanoids pathway, including 15 flavonoids, 9 phenolic acids and 5 lignans (Fig.5h). Comparatively, high Na_2SO_4 treatment increased 113 compounds from that pathway, including 52 flavonoids, 12 phenolic acids, 12 phenylpropanoids as well as 10 lignans. These included enrichment of important compounds such as 4-coumaroyl shikimate, 5-hydroxyferulate, procyanidol, catechin 3-O-(1-hydroxy-6-oxo-2-cyclohexene-1-carboxylate), 8-hydroxypinoresinol 4'-glucoside, guaicylglycerol-coniferyl ether, glucose-conjugated salicylic acid, and salicin. Six sphingolipids, including phytosphingosine and 4-hydroxysphinganine, were consistently depleted by both Na_2SO_4 concentrations, while 4 and 10 saccharides significantly reduced under moderate and high Na_2SO_4, respectively. In contrast, 8 nucleosides and 20 small peptides increased only under high Na_2SO_4, as did 8 pseudoalkaloids, 8 tryptophan alkaloids, 6 tyrosine alkaloids, 12 monoterpenoids, 11 steroids and 9 triterpenoids. In stems, moderate and high Na_2SO_4 treatments enriched 3 and 7 small peptides, such as aspartate and proline, while 7 and 8 small peptides were depleted, respectively. Additionally, 4 and 14 saccharides were depleted, including glucose and trehalose (Fig.5h), whereas 14 and 13 saccharides were enriched in leaves. Common, dose-responsive compounds in leaves were dominated by 49 shikimates/phenylpropanoids, encompassing enrichment of 9 cinnamic acid derivatives, 5 salicinoids and 4 other simple phenolic acids, 4 flavonols and 4 chalcons. Commonly regulated metabolites also included 25

alkaloids and 20 amino acids/peptides, with the enrichment of 7 pseudoalkaloids (5 purine and 2 pteridine alkaloids), 3 tryptophan alkaloids and 15 small peptides (Fig.5h).

A total of 179 DA compounds altered by one or both concentrations of Na_2SO_4 (12% of all Na_2SO_4 metabolomic changes) contained sulphur, corresponding to 101 distinct compounds. Roots significantly accumulated 13 and 45 sulphur compounds (S-compounds) under moderate and high Na_2SO_4 respectively, but significantly reduced 4 and 20 S-compounds (Fig.5i). Additionally in leaves, 36 S-compounds were increased under one or both Na_2SO_4 concentrations, compared to 11 depleted S-compounds. Shared enriched S-compounds included dicarboxylic acid such as 2-(2-sulfoethyl)propanedioic acid or polyamines, such as N'-hydroxy-5-(2-methoxyethyl-sulfamoylamino) pentanimidamide, as well as stilbenes, such as resveratrol 4-sulfate. High Na_2SO_4 depleted S-containing compounds ranged from small peptides, such as threonine to larger alkaloids such as $C_{19}H_{16}N_8O_5S$ (CHEMBL164867). Notably, a subgroup of 16 DA S-compounds were in the same structural cluster (Fig.5j).

4.4 Salix metabolomic response to NaCl treatment

Comparing metabolomes from controls with NaCl-treated willows, PCA revealed a significant separation between control and NaCl treatment in roots (*PERMANOVA*, p-value <0.05), partial overlap in stems (*PERMANOVA*, p-value < 0.05) and no observed separation in leaves (Fig.6a). NaCl treatment led to DA in 1,063 DA compounds, with 475 in roots, 481 in stems and 107 in leaves (Fig.6b). Among these, 768 DA compounds were unique to one organ, while 135 were shared to two or all organs (Fig.6c). Notably, 98 DA compounds were exclusively shared between roots and stems and 24 were significantly depleted in all three organs due to NaCl treatment.

Across all organs, NaCl-responsive metabolites comprised 213 DA compounds within the shikimates/phenylpropanoids pathway, 118 alkaloids, 88 carbohydrates, 74 amino acids/peptides, 59 terpenoids, 48 fatty acids and 12 polyketides (Fig.6d). While shikimates/phenylpropanoid pathway compounds were the most diverse, carbohydrates represented the highest proportional change within a pathway, constituting >33% of total carbohydrates (Supporting information – Fig.S7). This was driven by significant depletion in 28 carbohydrates across multiple organs, including glucose, fructose, sucrose and valienol 1,7-diphosphate, as well as organ-specific depletion of 36 carbohydrates (Fig.6e,f). Tricarboxylic acid cycle intermediates, such as malate, citrate, 2-oxoglutarate, were also depleted across the entire plant as well as phosphorylated compounds, such as phosphocholine, phosphonoacetaldehyde, 1,7-diphospho-1-epi-valienol and 2-C-methyl-D-erythritol-2,4-cyclodiphosphate (Supporting information – Fig.S8).

Within organs, leaves had a limited response to NaCl treatment (Fig.6b,c), but depleted compounds included 2-oxoglutarate, malate, aspartate and choline, while accumulated compounds included populoside C, (indol-3-yl)acetyl-myo-inositol L-arabinoside (IAA derivative) and spermidine (Supporting information – Tables S3,S7). Stems and roots had a larger metabolic response, markedly within the shikimate/phenylpropanoid pathway, altering 115 and 108 compounds respectively (Fig.6e). This large group of differentially abundant phenolic compounds was primarily associated to flavonoids, phenylpropanoids, lignans and phenolic acids (including salicinoids). While enriched flavonoids number were similar in stems and roots, 20 and 23 DA compounds respectively, stems had more depleted flavonoids than roots, with 23 and 10 DA compounds respectively (Fig.6h). Salicinoids were net enriched in both stems and roots (Fig.6h). Stems had significant enrichment of myricetin 3-O-glucoside, kaempferide 3-O-glucoside, procyanidol, salicin and grandidentatin, alongside the depletion of eriodictyol 7-glucuronide, luteolin 7-(6''-benzoylglucoside, ramontoside and a hydroxycyclohexen-oyl ester catechin derivative. In roots, populin, tremuloidin and benzoyl-β-D-glucoside were enriched, while (iso-)salicin, salicylic acid glucoside, grandidentatin, catechin, procyandin C, pleurostimin 7-glucoside were depleted. Additionally, 21 lignans and phenylpropanoids significantly accumulated in roots, contrasting stems, where 14 lignans and phenylpropanoids were depleted (Fig.6h).

A balanced pattern of metabolomic change was observed in nitrogen metabolism in response to NaCl treatment, with enrichment of 147 DA compounds and depletion of 133 DA compounds. This was particularly evident as 31 small peptides increased across all organs, including proline, tryptophan and glutathione, while 34 small peptides decreased, including acetylproline, threonine and arogenate (Fig.6g). Other increasing N-containing compounds included purine nucleosides like adenosine, alkaloids such as dihydrosanguinarine and kinetin-7-N-glucoside, as well as sphingolipids, such as phytosphingosine and sphinganine. Concurrently,

terpenoids were enriched, especially monoterpenoids, with 15 enriched monoterpenoids in stems and 13 in roots (Fig.6i,j).

4.5 Salix anion-specific metabolomics response to NaCl and Na_2SO_4 (at the same EC)

Comparing the 1,063 and 571 DA compounds altered by moderate NaCl and moderate Na_2SO_4 revealed 103 DA compounds commonly regulated in roots, 53 in stems and 7 in leaves (Fig.7a,b). These generalised salinity responsive metabolites included 23 shikimates/phenylpropanoids, 10 alkaloids, 10 carbohydrates, 9 terpenoids, 9 amino acids and peptides and 5 fatty acids (11 other and 70 unknown) (Fig.7b). Commonly enriched compounds included (indol-3-yl)acetyl-myo-inositol L-arabinoside and 2-phenylacetamide in leaves, proline, grandidentatin and fraxiresinol 1-O-glucoside (a lignan) in stems, 2-thioethylidenebis(phosphonic acid), delphinidin 3-O-(6''-O-malonyl)-beta-D-glucoside-3',5'-di-O-beta-D-glucosideand and syringin in roots. Commonly depleted compounds included glucose, trehalose in stems, D-altro-heptulose, glycerophophoglycerol, benzoyl-beta-D-glucoside and N-(4-(1-cyanocyclopentyl)phenyl)-2-((pyridin-4-ylmethyl)amino)nicotinamide in roots, as well as d-glycero-l-galacto-octulose in both stems and roots.

Anion specific responses included 764 DA compounds unique to moderate NaCl treatment and 391 DA compounds unique to the moderate Na_2SO_4. Both salt treatments induced the accumulation of salt-specific monoterpenoids, as well as phenolic compounds, including flavonoids, phenylpropanoids, and phenolic acids. Moreover, NaCl treatment led to a net decrease of saccharides and nucleosides, whereas Na_2SO_4 treatment resulted in their net accumulation (Fig.7c). An additional contrasting effect was observed with sphingolipids, with increased in NaCl but decreased Na_2SO_4 treated trees.

An anion-specific effect could also be observed when comparing change in constitutively produced compounds that were core (present and relatively stable between organs) and organ-specialised (significantly different between organs), but also in salt-induced compounds (not detected in controls). In both moderate salt treatments, roots primarily reduced root-specialised compounds rather than core compounds, while significantly enriched compounds were predominantly newly synthesised (salt-induced), rather than root-specialised or core compounds (Fig.7d). Similarly, in stems, reduced compounds were largely stem-specialised rather than core compounds under both salt types, however enriched compounds were predominantly stem-specialised under NaCl, comprising 53 enriched DA compounds as compared to 20 salt-induced and 23 core enriched DA compounds. Conversely, Na_2SO_4 treatment resulted in 2 stem-specialised, 5 salt-induced and 3 core enriched DA compounds. In leaves, NaCl treatment reduced 13 leaf-specialised and 4 core DA compounds while enriching 26 leaf-specialised, 20 salt-induced and 4 core DA compounds. In contrast, leaves treated with Na_2SO_4 decreased 22 leaf-specialised and 4 core compounds while increasing 5 leaf-specialised and 63 core compounds.

5 Discussion

5.1 Salix salinity tolerance response

Soil salinity levels are commonly categorised based on EC_e as slightly saline (2-4 dS m^{-1}), moderately saline (4-8 dS m^{-1}), and highly saline (>8 dS m^{-1}) (Corwin and Scudiero, 2019; FAO, 1988). Here, the comparison of non-saline control, moderately saline NaCl and Na_2SO_4, and highly saline Na_2SO_4 (Fig.2a) enabled capture of the anion-specific effects (Cl^- and SO_4^{2-}) and severity effects (moderate vs high Na_2SO_4) on willow (*Salix miyabeana* 'SX64').

Photosynthetic capacity and biomass productivity were maintained compared to water controls, even at high soil salinity levels of 9 dS m^{-1} (Fig.2c,d), supporting the suitability of willow for phytoremediation. This aligns with research by Hangs et al. (2011), reporting salinity tolerance in 37 willow varieties, where most cultivars could tolerate moderate soil salinity and the most salt-tolerant cultivars maintained yield under high soil salinity. Leaf moisture content increased under moderate salinity, alongside a >35% reduction of stomatal conductance (Fig.2e). This indicates reduced transpiration accompanied by osmotic adjustment to sustain turgor, potentially mitigating ion toxicity through absorbed salt dilution (Munns et al., 2020b; Nguyen et al., 2017). However, subsequent lower leaf moisture content suggests this water balance might not be maintained as salinity severity increase (Fig.2d).

402 Salt treatments did not reduce the acquisition of essential nutrients and even increased potassium uptake
403 alongside salt ions, although these ions were selectively partitioned (Fig.3). Sodium accumulation was
404 predominantly restricted to the roots and influx did not increase linearly with external concentration,
405 suggesting a robust sodium exclusion mechanism (Fig.3a). Such exclusion can occur through root cell wall Na^+
406 binding (Byrt et al., 2018) or competing uptake of K^+ (Hauser and Horie, 2010), as proposed in the salt tolerant
407 *Salix interior* (Major et al., 2017) and *Salix eriocephala* 'LAR' (Huang et al., 2023). In contrast, the high chloride
408 uptake and transport throughout the plant (Fig.3) can be facilitated by passive anion channels (Skerrett and
409 Tyerman, 1994), resulting in leaf chloride concentrations here reaching the upper optimal level for non-
410 halophytes (~30-560 µmol(Cl) g_{DW}^{-1} (Geilfus, 2018)). This accumulation, coupled with increased leaf water
411 content, suggests that Cl^- may serve as a readily available osmolyte, potentially conferring osmotic benefits
412 similar to those observed in *Nicotiana tabacum* (Franco-Navarro et al., 2016). However, given that cytosolic
413 chloride toxicity is thought to occur at concentrations of 5-20 mmol(Cl) L(cytosol)$^{-1}$ (Teakle and Tyerman, 2010),
414 the accumulated Cl^- may also require compartmentalisation into vacuoles, apoplasts, or older leaves to
415 mitigate cellular damage and optimise metabolic burden. In comparison to chloride, sulphate uptake was more
416 constrained but still resulted in increased transport throughout the plant, where it was either stored as SO_4^{2-}
417 or metabolised into organic sulphur compounds.

418 The maintenance of biomass yields despite reduced stomatal conductance, which can lead to decreased carbon
419 assimilation (Munns et al., 2020a), suggests effective metabolic plasticity and ion management strategies,
420 making this experimental system suitable for assessing willow metabolomic tolerance mechanisms without the
421 confounding metabolic effects associated with severe salt-induced physiological damage.

422 ***5.2 High organ-specific diversity in the Salix metabolome***

423 Untargeted metabolomic analysis of control trees revealed substantial diversity across the three main
424 vegetative organs (roots, stems and leaves), with over 5,000 compounds detected, approximately 62% of which
425 could be annotated at confidence levels 1-3 (Sumner et al., 2007), providing a detailed overview of the willow
426 metabolome at whole plant scale (Fig.4). Previous metabolomic studies in single organs of *Salix* have captured
427 up to 1,639 metabolites in bark (J. Zhou et al., 2022), 2,735 (Kaling et al., 2015), 600 (Jia et al., 2020) and 2,440
428 (Aliferis et al., 2015) metabolites in leaves, and 800 metabolites in roots (Xia et al., 2021). By integrating
429 analyses of multiple plant organs, a group of common metabolites across organs were identified, representing
430 26% of metabolomic diversity and over 70% of the putative abundance (estimated from peak area) (Fig.4d). Of
431 these, 287 metabolites had stable abundance across organs and represent its potential plant-wide basal, or
432 "core", metabolism (Fig.4f); a recent metabolomic concept that can also denote evolutionarily conserved
433 metabolites across species (Drapal et al., 2022; Dussarrat et al., 2022; McLaughlin et al., 2023). Many of these
434 core metabolites were associated with central pathways like glycolysis, TCA cycle derivatives, and amino acid
435 metabolism, reflecting primary metabolism across plant tissues. Others included bioactive phenolics found at
436 high levels in Salicaceae, such as characteristic salicylates (e.g. salicin, salicortin) associated to antioxidant,
437 antimicrobial and anti-herbivory functions in willow (Boeckler et al., 2011; Brereton et al., 2017; Meier et al.,
438 1988; Pobłocka-Olech et al., 2007; Tyśkiewicz et al., 2019; Volf et al., 2015).

439 Beyond these common metabolites, willow organs had clear metabolic differences (Fig.4g). Leaves contained
440 the most diverse metabolome, aligning with leaf function as a source of complex photosynthates. The leaf
441 metabolome included diverse terpenoids involved in light harvesting, development, defence, and signalling
442 (Pichersky and Raguso, 2018). Stems accumulated lignans and phenylpropanoids, reflecting woody tissue
443 functions of structure and storage (Boeckler et al., 2011; Köhler et al., 2020). Additionally, the metabolome of
444 stems had a large overlap with both leaves and roots, underscoring their function as conduits for biochemical
445 transport and dialog between aerial and belowground processes (Fig.4d). Comparatively, despite critical
446 functions of water and nutrient absorption, exudation, anchoring structure and storage, roots had the lowest
447 metabolic diversity (Fig.4a,b). Roots were enriched in saccharides and flavonoids, thought to mediate soil
448 interactions like microbial symbiosis (Endo et al., 2021), metal tolerance (Osawa et al., 2011), nutrient uptake
449 (Cesco et al., 2012) and root architecture (Buer et al., 2010). The root metabolome was also distinctly richer in
450 polar metabolites (Supporting information – Fig.S6) which can more readily diffuse through the soil
451 environment within the water vector and could therefore play a role as exudates involved in shaping the
452 rhizospheric biotic (Sasse et al., 2018) and abiotic (Badri and Vivanco, 2009) environment.

These distinct metabolomes reflect the different physiological roles of each organ, describing different metabolic activity and degree of functional specialisation (Li et al., 2016) as well as serving as a baseline to enable understanding of key responses to stimuli such as salt stress.

5.3 Sulphate salt induces dose-dependent metabolomic responses in Salix

Sulphate salinity induced extensive organ-specific metabolic reprogramming (Fig.5a-d,h), affecting 10% and 16% of all metabolites at moderate and high concentrations, respectively. Doubling the Na_2SO_4 concentration in soil resulted in a twofold increase of metabolic changes in roots, but more limited responses in stems and leaves. This localisation of metabolic response to the roots, which serve as the primary defence barrier against excess ions and osmotic stress, is likely decisive in mitigating salinity stress impact aboveground. Notably, consistent levels of salt ion uptake and accumulation despite increased soil salinity indicate effective ion management (Fig.3), allowing leaves to maintain similar adaptative metabolomic strategies under both sulphate salt treatments (Fig.5f,g). Previous studies reported sulphate salt tolerance in willows (Huang et al., 2020) associated with ion imbalance restriction to roots, similarly preventing physiological impact on leaves at moderate salinity levels.

In roots, Na_2SO_4 dose differentially effected shikimates/phenylpropanoids, with a reduction of flavonoids, phenolic acids and lignans under moderate level, contrasting their net increase under higher sulphate salinity (Fig.5h). This may indicate a developmental slowdown under mild stress, superseded by a required metabolic burst under more severe salinity levels. The lower osmotic potential associated with higher salinity likely drove the accumulation of lignans (Fig.5h) to enhance structural protection (as lignin precursors) and cavitation protection (Reyt et al. 2021), while accumulation of antioxidative flavonoids can enhance secondary oxidative stress tolerance (Nakabayashi et al., 2014). Under high Na_2SO_4, the sugar donor UDP-D-galactose significantly increased alongside phenolics, indicating a disruption in glycosylation and flavonoid bioactivity regulation (Xiao et al., 2014), while increases in iridoid monoterpenoids, such as lamiide, can prevent lipid peroxidation to protect cell membrane integrity (Delaporte et al., 2002). The high diversity of salt-responsive metabolites captured here implies additional functions beyond ROS scavenging, likely contributing to the observed Na_2SO_4 stress tolerance. Moreover, the reduction in sphingolipids, which regulate ions through early sensing and signalling, could limit salt uptake below toxic thresholds (Jiang et al., 2019; Liu et al., 2022), coherent with depletion of the essential precursor octanoyl-CoA (Neess et al., 2015; Sonar et al., 2020).

Primary metabolites declined in stems under both sulphur salt concentrations, including reductions in small peptides, saccharides, and nucleosides (Fig.5h). A slowdown of developmental processes and primary metabolism would be expected under salt stress, although there was no accompanying (short-term) impairment to total biomass production (Fig.2c). The comparatively limited disruption of secondary metabolites in stems indicates maintenance of homeostasis and primary resource allocation to support root functions, effectively restricting salt stress propagation.

In leaves, the salt-responsive metabolites were broadly shared between both Na_2SO_4 levels, characterised by dose-dependent accumulation, including saccharides, small peptides and precursors of phenolic compounds (Fig.5f,g). Again, illustrating the buffering role of roots in protecting essential carbon fixation functions and energy-related compound production, even under severe salt exposure.

An increase of sulphur-containing compound synthesis under SO_4^{2-} treatment and upregulation of sulphur assimilation and transport pathways is a characterised plant adaptation mechanism to effectively utilise excess SO_4^{2-} (Buchner et al., 2004; Davidian and Kopriva, 2010). Here, a substantial enrichment of small peptides occurred in roots under sulphur salinity (Fig.5h), with around half incorporating sulphur. This accumulation of sulphur-containing compounds was consistent throughout the plant at both concentrations (Fig.5i) and was predominantly cysteine and glutathione-based small peptides and some fatty acyl thioesters and alkaloids. The integration of sulphate ions into organic sulphur-containing compounds has the potential to reduce ion imbalance *in planta* during salt stress and could represent a tolerance mechanism in willow. Moreover, the increase of structurally related compounds here (Fig.5i), although their functional information is limited, suggests activation of a bespoke, yet-to-be-described, metabolic response to Na_2SO_4. Watanabe et al. (2019) highlighted a need for integrated sulphur-omics to overcome this shortfall in functional understanding of sulphur-containing molecules in plants, of particular relevance to salinity tolerant non-model organisms such as willow.

5.4 Salt anions shape Salix metabolomic tolerance responses

The salt response across all treatments involved an extensive proportion of the metabolome (28% of metabolites), reflecting the highly plastic nature of plant metabolism under environmental challenge. While activation of the calcium sensing signalling pathway by Na^+ (Munns and Tester, 2008) and disruption of the Na^+/K^+ ratio (Zhang et al., 2018) are commonly considered to trigger salt responses in plants, anion driven metabolomic responses have been less well explored. Comparison of metabolomic responses to moderate NaCl and Na_2SO_4 treatments here, at equivalent soil electroconductivity and sodium concentrations, revealed only 3% of metabolites were consistently responsive, highlighting extensive anion-specific changes (Fig.7).

The common, or generalised, salt metabolite changes were asymmetrically distributed across organs, with ~15-fold more generalised salt responses in roots than in leaves (Fig.7b). These represent common metabolic strategies to tolerate (anion agnostic) osmotic stress in roots at the root-soil interface and restrict sodium translocation, while leaves might be more susceptible to the (anion dependent) ion toxicity of translocated Cl^- and SO_4^{2-}. The generalised salt response included common accumulation of the phenylpropanoid precursor 2-phenylacetamide in leaves (a salt biomarker in the euhalophyte *Suaeda salsa* (Bao et al., 2023)), protective molecules in stems such as the anthocyanin ternatin C5 (Kovinich et al., 2015) and a highly antioxidative coumaric acid conjugate of salicin, grandidentatin (Si et al., 2009), as well as potential cell wall structural components in roots, such as the monolignol precursors syringin.

NaCl treatment, unlike Na_2SO_4, induced a comparatively small metabolomic response in leaves (Fig.6a-c). Of the limited responses, a significant accumulation of spermidine, a polyamine known for its acid- and ROS-neutralising properties, could help protect cell membranes, reduce chlorophyll loss and leaf senescence (Gill and Tuteja, 2010b). The auxin conjugate, (indol-3-ylacetyl)-myo-inositol L-arabinoside, also increased, suggesting oxidative stress specific developmental regulation (Bajguz and Piotrowska, 2009; Ludwig-Müller, 2011). A larger change under NaCl salt exposure was the reconfiguration of carbon resources through the shikimate/phenylpropanoids pathway (Fig.6d,h). Specifically, lignans and phenylpropanoids had organ-specific responses: substantial accumulation in roots and significant depletion in stems (Fig.6h). As major lignin precursors, these lignan and phenylpropanoid dynamics could represent the expected structural adaptations within the roots and stems. In particular, lignin deposition can act as a barrier regulating ion uptake and translocation to aerial parts (Byrt et al., 2018; Neves et al., 2010; Reyt et al., 2021).

Flavonoids, whose antioxidative capacity can facilitate localised neutralisation of ROS (Nakabayashi et al., 2014), also had marked organ-specific responses, with substantial accumulation in roots and variable regulation in the stems (Fig.6h). As flavonoids, phenolic acids, lignans and phenylpropanoids all derive from the same substrates (phenylalanine and the pivotal intermediate cinnamic acid), the organ-specific shift suggests a coordinated metabolic response promoting defence in the directly exposed roots while simultaneously restricting the availability and energy expense of these compounds in the stems. By comparison, moderate Na_2SO_4 did not induce similar extensive accumulation of phenolic compounds in roots or stems but this response was triggered under higher Na_2SO_4 concentration.

Accumulation of osmoprotectants under salt stress is one of the most prevalent and well-described adaptive strategies to reduce cell osmotic potential and stabilise cellular components (D'Amelia et al., 2018; Yang and Guo, 2018). Surprisingly, except for stem proline enrichment under both NaCl and Na_2SO_4, the levels of expected organic osmoprotectants, namely hydrophilic and low molecular weight sugars, polyamines or amino acids, were largely reduced in roots and stems under NaCl while accumulating in leaves under Na_2SO_4, more distal to the primary site of osmotic stress (Fig.5h, Fig.6f,g and Fig.7c). This response contrasts salt-tolerant poplars which can accumulate soluble sugars as a tolerance mechanism (Jouve et al., 2004; Watanabe et al., 2000) and might be a distinct strategy used by *S. miyabeana* to mitigate osmotic stress through the uptake of inorganic ions, including root restricted Na^+ and anions (Cl^- and SO_4^{2-}) translocation to leaves. Similarly, Ottow et al. (2005) reported preferential sodium uptake by *Populus euphratica*, where Na^+ served as a readily-available osmoprotectant stored in the apoplast or bound in the cell wall, alongside reduced calcium and soluble carbohydrate levels.

The anion-dependent regulation pattern of osmoprotectants also reflected broader differing metabolic adjustments within central metabolism. Although reduction of stomatal conductance was similar between both salts and photosystem II efficiency (Φ_{PSII}) preserved (Fig.2), the impact on foliar glucose and energy-related compounds was distinct. NaCl induced the plant-wide reduction of glucose and multiple TCA cycle

556 intermediates (Supporting information – Fig.S8), representing impaired photosynthetic carbon fixation and
557 decreased flux through glycolysis and the TCA cycle, limiting mitochondrial respiration and overall energy
558 supply. A similar reconfiguration of resources and metabolic processes has been observed under salt stress in
559 barley roots (Wu et al., 2013), where glycolysis was inhibited, and in *Arabidopsis thalia* (Hartmann et al., 2015),
560 where a shift to non-oxidative fermentative energy metabolism can occur. This was coupled with reduced
561 levels of small peptides, nucleosides and other simple carbohydrates like fructose and sucrose in stems and
562 roots (Fig.6f,g and Fig.7c), possibly driven by increased carbon demand for secondary metabolism involved in
563 salt stress tolerance. By comparison, Na_2SO_4 induced an increase of glucose in leaves (Supporting information
564 – Fig.S8), alongside an accumulation of saccharides, small peptides and nucleosides, consistent even under
565 high Na_2SO_4. This suggests that willow can sustain chemical energy production in leaves in the presence of
566 sulphate, unlike with chloride, and plant-wide production of salt-tolerance supporting metabolites,
567 underscoring the importance of understanding anion toxicity in salt tolerance and implicating organic
568 compound sulphate incorporation in prevention of ionic imbalance. As an example, the accumulation of
569 sulphur-containing metabolites (Fig.5i,j), including 2,3-di-O-sulfopropylglucose, aligns with the known
570 mechanism of sugar sulphonation that promotes salt tolerance through ion regulation, osmotic tolerance, and
571 cell wall integrity in algae (Aquino et al., 2011).

572 Both chloride and sulphate salts activated the terpenoid pathway (Supporting information – Fig.S9), known to
573 mitigate salt stress in mangroves (Basyuni et al., 2009). NaCl induced significant accumulation of terpenoids
574 from the chloroplastic methylerythritol phosphate (MEP) pathway across the whole plant, including
575 diterpenoids as well as iridoid and secoiridoid monoterpenoids, reflecting transcriptomic changes observed in
576 salt-tolerant poplar (Chen et al., 2018). Na_2SO_4 treatment similarly enriched terpenoids through the MEP
577 pathway, but also activated the cytoplasmic mevalonate pathway in roots, also linked to salt tolerance in poplar
578 (Wei et al., 2020). This sulphate-salt-associated activation of the mevalonate pathway increased with higher
579 Na_2SO_4 levels, including enrichment of the hormone precursor abscisic aldehyde in roots and leaves. This
580 suggests an adaptive stress response where willows are positioned to quickly synthesise ABA, signalling
581 stomatal closure, root architecture changes, and osmoprotectant accumulation (Ryu and Cho, 2015), with
582 ABA-aldehyde oxidase mediated regulation. In contrast, ABA precursor enrichment was not observed with
583 NaCl, indicating chloride ion interference with signalling that may leave willows more vulnerable to salt stress.

584 Overall, willow responded to salt stress by modulating both core and organ-specialised metabolites (Fig.4 and
585 Fig.7d). Within each organ, there was a tendency for greater depletion of organ-specialised compounds, over
586 core metabolites, indicating higher resilience of core metabolism under salt stress (Fig.7d). Contrasting this,
587 Na_2SO_4 treatment resulted in the enrichment of core metabolites in leaves, while NaCl enriched organ-
588 specialised compounds. This anion-specific difference further highlights the nuanced metabolic mechanisms
589 deployed to face distinct salt stress conditions.

590 **6 Conclusion**

591 Untargeted metabolomics uncovered extremely high diversity of metabolites in willow, the majority of which
592 represent organ-specialised metabolites aligned with distinct physiological functions, but which also include
593 over 250 putative plant-wide stable, or core, metabolites. The leaves had the highest metabolite diversity, but
594 when subjected to different saline soil conditions, roots, as the frontline of exposure, had the most extensive
595 biochemical response, mitigating ion toxicity and osmotic pressure changes to enable plant tolerance.
596 Accompanying this was plant-wide reallocation of energy and metabolic resources, coupled with prioritisation
597 of antioxidant flavonoids, able to protect vulnerable leaf photosynthetic functions, constituting the signature
598 of a general willow salt response. However, the largely specialised nature of this response revealed that *in*
599 *planta*, salt anion type becomes an increasingly stronger discriminating force of metabolomic profile when
600 moving from roots to leaves. Indeed, the metabolic adjustment differed extensively in leaves, where Na_2SO_4
601 induces key components of the core metabolome to mitigate complex osmotic and toxic stress even as soil
602 salinity increases, whereas NaCl induces more organ-specialised metabolic tools. Salinity levels in agriculture
603 are currently categorised by soil EC, however, given the substantial anion-dependent differences observed in
604 plant metabolic responses, soil EC measurement might be insufficient to reflect the diversity of soil salinity
605 types, their actual osmotic potential, as well as the anion-specific plant metabolic toolkit necessary for plant
606 salt tolerance.

7 Declaration of Competing Interest

The authors declare that there is no conflict of interest.

8 Acknowledgements

We gratefully acknowledge the financial support provided from NSERC Discovery Grants (RGPIN-2017-05452 and RGPIN-2023-04863), Natural Resources Canada Forest Innovation Program Grant (CWFC1718-018 and CWFC1920-104), ECCC Environmental Damage Fund (EDF-PQ-2020b012), MITACS (IT23193), and the UCD Ad Astra Award Program. A special thank you is extended to Ariane Lafrenière, Marc-Olivier Brunette and Bruno Guerrier for their kind and effective support during harvest, and to Allan Harms from NRAL, University of Alberta, for his valuable expertise and sympathy.

9 Data availability statement

The data that supports the findings of this study are available in the supporting information of this article and on GNPS-MassIVE online dataset repository.

10 References

Abdelgadir, E.M., Oka, M., Fujiyama, H., 2005. Characteristics of nitrate uptake by plants under salinity. J. Plant Nutr. 28, 33–46. https://doi.org/10.1081/PLN-200042156

Abreu, M., Silva, L., Ribeiro, B., Ferreira, A., Alves, L., Paixão, S.M., Gouveia, L., Moura, P., Carvalheiro, F., Duarte, L.C., Fernando, A.L., Reis, A., Gírio, F., 2022. Low indirect land use change (ILUC) energy crops to bioenergy and biofuels: A review. Energies 15, 4348. https://doi.org/10.3390/en15124348

Aliferis, K.A., Chamoun, R., Jabaji, S., 2015. Metabolic responses of willow (*Salix purpurea* L.) leaves to mycorrhization as revealed by mass spectrometry and 1H NMR spectroscopy metabolite profiling. Front. Plant Sci. 6.

Alseekh, S., Aharoni, A., Brotman, Y., Contrepois, K., D'Auria, J., Ewald, J., C. Ewald, J., Fraser, P.D., Giavalisco, P., Hall, R.D., Heinemann, M., Link, H., Luo, J., Neumann, S., Nielsen, J., Perez de Souza, L., Saito, K., Sauer, U., Schroeder, F.C., Schuster, S., Siuzdak, G., Skirycz, A., Sumner, L.W., Snyder, M.P., Tang, H., Tohge, T., Wang, Y., Wen, W., Wu, S., Xu, G., Zamboni, N., Fernie, A.R., 2021. Mass spectrometry-based metabolomics: A guide for annotation, quantification and best reporting practices. Nat. Methods 18, 747–756. https://doi.org/10.1038/s41592-021-01197-1

Aquino, R.S., Grativol, C., Mourão, P.A.S., 2011. Rising from the sea: Correlations between sulfated polysaccharides and salinity in plants. PLOS ONE 6, e18862. https://doi.org/10.1371/journal.pone.0018862

Arif, Y., Singh, P., Siddiqui, H., Bajguz, A., Hayat, S., 2020. Salinity induced physiological and biochemical changes in plants: An omic approach towards salt stress tolerance. Plant Physiol. Biochem. 156, 64–77. https://doi.org/10.1016/j.plaphy.2020.08.042

Badri, D.V., Vivanco, J.M., 2009. Regulation and function of root exudates. Plant Cell Environ. 32, 666–681. https://doi.org/10.1111/j.1365-3040.2009.01926.x

Bajguz, A., Piotrowska, A., 2009. Conjugates of auxin and cytokinin. Phytochemistry 70, 957–969. https://doi.org/10.1016/j.phytochem.2009.05.006

Bao, J., Liu, Z., Ding, Z., Yisilam, G., Wang, Q., Tian, X., Bao, J., Liu, Z., Ding, Z., Yisilam, G., Wang, Q., Tian, X., 2023. Metabolomic analysis reveals key metabolites and metabolic pathways in *Suaeda salsa* under salt and drought stress. Funct. Plant Biol. https://doi.org/10.1071/FP23049

Basyuni, M., Baba, S., Inafuku, M., Iwasaki, H., Kinjo, K., Oku, H., 2009. Expression of terpenoid synthase mRNA and terpenoid content in salt stressed mangrove. J. Plant Physiol. 166, 1786–1800. https://doi.org/10.1016/j.jplph.2009.05.008

Bilek, M.A., Soolanayakanahally, R.Y., Guy, R.D., Mansfield, S.D., 2020. Physiological response of *Populus balsamifera* and *Salix eriocephala* to salinity and hydraulic fracturing wastewater: potential for phytoremediation applications. Int. J. Environ. Res. Public. Health 17, 7641. https://doi.org/10.3390/ijerph17207641

654 Boeckler, G.A., Gershenzon, J., Unsicker, S.B., 2011. Phenolic glycosides of the Salicaceae and their role as anti-
655 herbivore defenses. Phytochemistry, Plant-Insect Interactions 72, 1497–1509.
656 https://doi.org/10.1016/j.phytochem.2011.01.038
657 Brereton, N.J.B., Berthod, N., Lafleur, B., Pedneault, K., Pitre, F.E., Labrecque, M., 2017. Extractable phenolic
658 yield variation in five cultivars of mature short rotation coppice willow from four plantations in Quebec.
659 Ind. Crops Prod. 97, 525–535. https://doi.org/10.1016/j.indcrop.2016.12.049
660 Buchner, P., Takahashi, H., Hawkesford, M.J., 2004. Plant sulphate transporters: Co-ordination of uptake,
661 intracellular and long-distance transport. J. Exp. Bot. 55, 1765–1773.
662 https://doi.org/10.1093/jxb/erh206
663 Buer, C.S., Imin, N., Djordjevic, M.A., 2010. Flavonoids: New roles for old molecules. J. Integr. Plant Biol. 52,
664 98–111. https://doi.org/10.1111/j.1744-7909.2010.00905.x
665 Byrt, C.S., Munns, R., Burton, R.A., Gilliham, M., Wege, S., 2018. Root cell wall solutions for crop plants in saline
666 soils. Plant Sci. 269, 47–55. https://doi.org/10.1016/j.plantsci.2017.12.012
667 Cesco, S., Mimmo, T., Tonon, G., Tomasi, N., Pinton, R., Terzano, R., Neumann, G., Weisskopf, L., Renella, G.,
668 Landi, L., Nannipieri, P., 2012. Plant-borne flavonoids released into the rhizosphere: impact on soil bio-
669 activities related to plant nutrition. A review. Biol. Fertil. Soils 48, 123–149.
670 https://doi.org/10.1007/s00374-011-0653-2
671 Chambers, M.C., Maclean, B., Burke, R., Amodei, D., Ruderman, D.L., Neumann, S., Gatto, L., Fischer, B., Pratt,
672 B., Egertson, J., Hoff, K., Kessner, D., Tasman, N., Shulman, N., Frewen, B., Baker, T.A., Brusniak, M.-Y.,
673 Paulse, C., Creasy, D., Flashner, L., Kani, K., Moulding, C., Seymour, S.L., Nuwaysir, L.M., Lefebvre, B.,
674 Kuhlmann, F., Roark, J., Rainer, P., Detlev, S., Hemenway, T., Huhmer, A., Langridge, J., Connolly, B.,
675 Chadick, T., Holly, K., Eckels, J., Deutsch, E.W., Moritz, R.L., Katz, J.E., Agus, D.B., MacCoss, M., Tabb,
676 D.L., Mallick, P., 2012. A cross-platform toolkit for mass spectrometry and proteomics. Nat. Biotechnol.
677 30, 918–920. https://doi.org/10.1038/nbt.2377
678 Chan, K.X., Phua, S.Y., Van Breusegem, F., 2019. Secondary sulfur metabolism in cellular signalling and oxidative
679 stress responses. J. Exp. Bot. 70, 4237–4250. https://doi.org/10.1093/jxb/erz119
680 Chen, P., Zuo, L., Yu, X., Dong, Y., Zhang, S., Yang, M., 2018. Response mechanism in *Populus × euramericana*
681 cv. '74/76' revealed by RNA-seq under salt stress. Acta Physiol. Plant. 40, 96.
682 https://doi.org/10.1007/s11738-018-2676-x
683 Chen, S., Polle, A., 2010. Salinity tolerance of *Populus*. Plant Biol. 12, 317–333. https://doi.org/10.1111/j.1438-
684 8677.2009.00301.x
685 Corwin, D.L., Scudiero, E., 2019. Review of soil salinity assessment for agriculture across multiple scales using
686 proximal and/or remote sensors, in: Sparks, D.L., Sparks, D.L. (Eds.), Advances in Agronomy. pp. 1–130.
687 D'Amelia, L., Dell'Aversana, E., Woodrow, P., Ciarmiello, L.F., Carillo, P., 2018. Metabolomics for crop
688 improvement against salinity stress, in: Kumar, V., Wani, S.H., Suprasanna, P., Tran, L.-S.P., Kumar, V.,
689 Wani, S.H., Suprasanna, P., Tran, L.-S.P. (Eds.), Salinity Responses and Tolerance in Plants, Volume 2:
690 Exploring RNAi, Genome Editing and Systems Biology. Cham, pp. 267–287.
691 Davidian, J.-C., Kopriva, S., 2010. Regulation of sulfate uptake and assimilation—the same or not the same?
692 Mol. Plant 3, 314–325. https://doi.org/10.1093/mp/ssq001
693 De Vos, R.C., Moco, S., Lommen, A., Keurentjes, J.J., Bino, R.J., Hall, R.D., 2007. Untargeted large-scale plant
694 metabolomics using liquid chromatography coupled to mass spectrometry. Nat. Protoc. 2, 778–791.
695 https://doi.org/10.1038/nprot.2007.95
696 Deinlein, U., Stephan, A.B., Horie, T., Luo, W., Xu, G., Schroeder, J.I., 2014. Plant salt-tolerance mechanisms.
697 Trends Plant Sci. 19, 371–379. https://doi.org/10.1016/j.tplants.2014.02.001
698 Delaporte, R.H., Sánchez, G.M., Cuellar, A.C., Giuliani, A., Palazzo de Mello, J.C., 2002. Anti-inflammatory
699 activity and lipid peroxidation inhibition of iridoid lamiide isolated from *Bouchea fluminensis* (Vell.)
700 Mold. (Verbenaceae). J. Ethnopharmacol. 82, 127–130. https://doi.org/10.1016/S0378-
701 8741(02)00181-2
702 Dick, W.A., Kost, D., Chen, L., 2008. Availability of sulfur to crops from soil and other sources, in: Sulfur: A
703 Missing Link between Soils, Crops, and Nutrition. John Wiley & Sons, Ltd, pp. 59–82.
704 https://doi.org/10.2134/agronmonogr50.c5
705 Dimitriou, I., Aronsson, P., 2005. Willows for energy and phytoremediation in Sweden. Unasylva 56.
706 Drapal, M., Enfissi, E.M.A., Fraser, P.D., 2022. The chemotype core collection of genus *Nicotiana*. Plant J. 110,
707 1516–1528. https://doi.org/10.1111/tpj.15745

Dührkop, K., Fleischauer, M., Ludwig, M., Aksenov, A.A., Melnik, A.V., Meusel, M., Dorrestein, P.C., Rousu, J., Böcker, S., 2019. SIRIUS 4: a rapid tool for turning tandem mass spectra into metabolite structure information. Nat. Methods 16, 299–302. https://doi.org/10.1038/s41592-019-0344-8

Dührkop, K., Nothias, L.-F., Fleischauer, M., Reher, R., Ludwig, M., Hoffmann, M.A., Petras, D., Gerwick, W.H., Rousu, J., Dorrestein, P.C., Böcker, S., 2021. Systematic classification of unknown metabolites using high-resolution fragmentation mass spectra. Nat. Biotechnol. 39, 462–471. https://doi.org/10.1038/s41587-020-0740-8

Dussarrat, T., Prigent, S., Latorre, C., Bernillon, S., Flandin, A., Díaz, F.P., Cassan, C., Van Delft, P., Jacob, D., Varala, K., Joubes, J., Gibon, Y., Rolin, D., Gutiérrez, R.A., Pétriacq, P., 2022. Predictive metabolomics of multiple Atacama plant species unveils a core set of generic metabolites for extreme climate resilience. New Phytol. 234, 1614–1628. https://doi.org/10.1111/nph.18095

Endo, I., Kobatake, M., Tanikawa, N., Nakaji, T., Ohashi, M., Makita, N., 2021. Anatomical patterns of condensed tannin in fine roots of tree species from a cool-temperate forest. Ann. Bot. 128, 59–71. https://doi.org/10.1093/aob/mcab022

Evelin, H., Kapoor, R., Giri, B., 2009. Arbuscular mycorrhizal fungi in alleviation of salt stress: a review. Ann. Bot. 104, 1263–1280. https://doi.org/10.1093/aob/mcp251

FAO, 2015. Status of the world's soil resources: Main report.

FAO, 1988. Salt-affected soils and their management (No. FAO Soils Bulletin 39).

Franco-Navarro, J.D., Brumós, J., Rosales, M.A., Cubero-Font, P., Talón, M., Colmenero-Flores, J.M., 2016. Chloride regulates leaf cell size and water relations in tobacco plants. J. Exp. Bot. 67, 873–891. https://doi.org/10.1093/jxb/erv502

Geilfus, C.-M., 2018. Chloride: from nutrient to toxicant. Plant Cell Physiol. 59, 877–886. https://doi.org/10.1093/pcp/pcy071

Genty, B., Briantais, J.-M., Baker, N.R., 1989. The relationship between the quantum yield of photosynthetic electron transport and quenching of chlorophyll fluorescence. Biochim. Biophys. Acta BBA - Gen. Subj. 990, 87–92. https://doi.org/10.1016/S0304-4165(89)80016-9

Gil-de-la-Fuente, A., Godzien, J., Saugar, S., Garcia-Carmona, R., Badran, H., Wishart, D.S., Barbas, C., Otero, A., 2019. CEU Mass Mediator 3.0: A metabolite annotation tool. J. Proteome Res. 18, 797–802. https://doi.org/10.1021/acs.jproteome.8b00720

Gill, S.S., Tuteja, N., 2010a. Reactive oxygen species and antioxidant machinery in abiotic stress tolerance in crop plants. Plant Physiol. Biochem. 48, 909–930. https://doi.org/10.1016/J.PLAPHY.2010.08.016

Gill, S.S., Tuteja, N., 2010b. Polyamines and abiotic stress tolerance in plants. Plant Signal. Behav. 5, 26–33. https://doi.org/10.4161/psb.5.1.10291

Gonzalez, E., Pitre, F.E., Pagé, A.P., Marleau, J., Guidi Nissim, W., St-Arnaud, M., Labrecque, M., Joly, S., Yergeau, E., Brereton, N.J.B., 2018. Trees, fungi and bacteria: tripartite metatranscriptomics of a root microbiome responding to soil contamination. Microbiome 6, 53. https://doi.org/10.1186/s40168-018-0432-5

Gupta, B., Huang, B., 2014. Mechanism of salinity tolerance in plants: physiological, biochemical, and molecular characterization. Int. J. Genomics 2014, 701596–701596. https://doi.org/10.1155/2014/701596

Hangs, R.D., Schoenau, J.J., Van Rees, K.C.J., Steppuhn, H., 2011. Examining the salt tolerance of willow (*Salix* spp.) bioenergy species for use on salt-affected agricultural lands. Can. J. Plant Sci. 91, 509–517. https://doi.org/10.4141/cjps10135

Hartmann, L., Pedrotti, L., Weiste, C., Fekete, A., Schierstaedt, J., Göttler, J., Kempa, S., Krischke, M., Dietrich, K., Mueller, M.J., Vicente-Carbajosa, J., Hanson, J., Dröge-Laser, W., 2015. Crosstalk between two bZIP signaling pathways orchestrates salt-induced metabolic reprogramming in *Arabidopsis* roots. Plant Cell 27, 2244–2260. https://doi.org/10.1105/tpc.15.00163

Hauser, F., Horie, T., 2010. A conserved primary salt tolerance mechanism mediated by HKT transporters: a mechanism for sodium exclusion and maintenance of high K+/Na+ ratio in leaves during salinity stress. Plant Cell Environ. 33, 552–565. https://doi.org/10.1111/j.1365-3040.2009.02056.x

Hawkins, C., Ginzburg, D., Zhao, K., Dwyer, W., Xue, B., Xu, A., Rice, S., Cole, B., Paley, S., Karp, P., Rhee, S.Y., 2021. Plant Metabolic Network 15: A resource of genome-wide metabolism databases for 126 plants and algae. J. Integr. Plant Biol. 63, 1888–1905. https://doi.org/10.1111/jipb.13163

He, H., Tang, W., Wang, W., Crits-Christoph, P., 2014. Structural zeroes and zero-inflated models. Shanghai Arch. Psychiatry 26, 236–242. https://doi.org/10.3969/j.issn.1002-0829.2014.04.008

Huang, X., Hefer, C.A., Soolanayakanahally, R.Y., Guy, R.D., Mansfield, S.D., 2023. The overlooked ion: Unraveling the effects of magnesium-specific toxicity on willows under sulphate salinity. Environ. Exp. Bot. 105634. https://doi.org/10.1016/j.envexpbot.2023.105634

Huang, X., Soolanayakanahally, R.Y., Guy, R.D., Shunmugam, A.S.K., Mansfield, S.D., 2020. Differences in growth and physiological and metabolic responses among Canadian native and hybrid willows (*Salix* spp.) under salinity stress. Tree Physiol. 40, 652–666. https://doi.org/10.1093/treephys/tpaa017

Huber, F., Ridder, L., Verhoeven, S., Spaaks, J.H., Diblen, F., Rogers, S., Hooft, van der J.J.J., 2021. Spec2Vec: Improved mass spectral similarity scoring through learning of structural relationships. PLOS Comput. Biol. 17, e1008724. https://doi.org/10.1371/journal.pcbi.1008724

Ifuku, K., 2015. Localization and functional characterization of the extrinsic subunits of photosystem II: an update. Biosci. Biotechnol. Biochem. 79, 1223–1231. https://doi.org/10.1080/09168451.2015.1031078

Janz, D., Lautner, S., Wildhagen, H., Behnke, K., Schnitzler, J.-P., Rennenberg, H., Fromm, J., Polle, A., 2012. Salt stress induces the formation of a novel type of 'pressure wood' in two *Populus* species. New Phytol. 194, 129–141. https://doi.org/10.1111/j.1469-8137.2011.03975.x

Jia, H., Wang, L., Li, J., Sun, P., Lu, M., Hu, J., 2020. Comparative metabolomics analysis reveals different metabolic responses to drought in tolerant and susceptible poplar species. Physiol. Plant. 168, 531–546. https://doi.org/10.1111/ppl.13036

Jiang, Z., Zhou, X., Tao, M., Yuan, F., Liu, L., Wu, F., Wu, X., Xiang, Y., Niu, Y., Liu, F., Li, C., Ye, R., Byeon, B., Xue, Y., Zhao, H., Wang, H.-N., Crawford, B.M., Johnson, D.M., Hu, C., Pei, C., Zhou, W., Swift, G.B., Zhang, H., Vo-Dinh, T., Hu, Z., Siedow, J.N., Pei, Z.-M., 2019. Plant cell-surface GIPC sphingolipids sense salt to trigger Ca2+ influx. Nature 572, 341–346. https://doi.org/10.1038/s41586-019-1449-z

Jouve, L., Hoffmann, L., Hausman, J.-F., 2004. Polyamine, carbohydrate, and proline content changes during salt stress exposure of Aspen (*Populus tremula* L.): Involvement of oxidation and osmoregulation metabolism. Plant Biol. 6, 74–80. https://doi.org/10.1055/s-2003-44687

Kaling, M., Kanawati, B., Ghirardo, A., Albert, A., Winkler, J.B., Heller, W., Barta, C., Loreto, F., Schmitt-Kopplin, P., Schnitzler, J.-P., 2015. UV-B mediated metabolic rearrangements in poplar revealed by non-targeted metabolomics. Plant Cell Environ. 38, 892–904. https://doi.org/10.1111/pce.12348

Karpievitch, Y.V., Nikolic, S.B., Wilson, R., Sharman, J.E., Edwards, L.M., 2014. Metabolomics data normalization with EigenMS. PloS One 9, e116221. https://doi.org/10.1371/journal.pone.0116221

Kim, H.W., Wang, M., Leber, C.A., Nothias, L.-F., Reher, R., Kang, K.B., van der Hooft, J.J.J., Dorrestein, P.C., Gerwick, W.H., Cottrell, G.W., 2021. NPClassifier: A deep neural network-based structural classification tool for natural products. J. Nat. Prod. 84, 2795–2807. https://doi.org/10.1021/acs.jnatprod.1c00399

Köhler, A., Förster, N., Zander, M., Ulrichs, C., 2020. Compound-specific responses of phenolic metabolites in the bark of drought-stressed *Salix daphnoides* and *Salix purpurea*. Plant Physiol. Biochem. 155, 311–320. https://doi.org/10.1016/j.plaphy.2020.07.004

Kovinich, N., Kayanja, G., Chanoca, A., Otegui, M.S., Grotewold, E., 2015. Abiotic stresses induce different localizations of anthocyanins in *Arabidopsis*. Plant Signal. Behav. 10, e1027850. https://doi.org/10.1080/15592324.2015.1027850

Li, D., Heiling, S., Baldwin, I.T., Gaquerel, E., 2016. Illuminating a plant's tissue-specific metabolic diversity using computational metabolomics and information theory. Proc. Natl. Acad. Sci. 113, E7610–E7618. https://doi.org/10.1073/pnas.1610218113

Liu, Y., Wang, L., Li, X., Luo, M., 2022. Detailed sphingolipid profile responded to salt stress in cotton root and the GhIPCS1 is involved in the regulation of plant salt tolerance. Plant Sci. 316, 111174. https://doi.org/10.1016/j.plantsci.2021.111174

Llanes, A., Bertazza, G., Palacio, G., Luna, V., 2013. Different sodium salts cause different solute accumulation in the halophyte *Prosopis strombulifera*. Plant Biol. 15, 118–125. https://doi.org/10.1111/j.1438-8677.2012.00626.x

Ludwig-Müller, J., 2011. Auxin conjugates: Their role for plant development and in the evolution of land plants. J. Exp. Bot. 62, 1757–1773. https://doi.org/10.1093/jxb/erq412

Major, J.E., Mosseler, A., Malcolm, J.W., 2017. *Salix* species variation in leaf gas exchange, sodium, and nutrient parameters at three levels of salinity. Can. J. For. Res. 47, 1045–1055. https://doi.org/10.1139/cjfr-2017-0028

McLaughlin, S., Zhalnina, K., Kosina, S., Northen, T.R., Sasse, J., 2023. The core metabolome and root exudation dynamics of three phylogenetically distinct plant species. Nat. Commun. 14, 1649. https://doi.org/10.1038/s41467-023-37164-x

Meier, B., Julkunen-Tiitto, R., Tahvanainen, J., Sticher, O., 1988. Comparative high-performance liquid and gas-liquid chromatographic determination of phenolic glucosides in *Salicaceae* species. J. Chromatogr. A 442, 175–186. https://doi.org/10.1016/S0021-9673(00)94467-4

Mirck, J., Zalesny, R.S., 2015. Mini-review of knowledge gaps in salt tolerance of plants applied to willows and poplars. Int. J. Phytoremediation 17, 640–650. https://doi.org/10.1080/15226514.2014.950414

Munns, R., 2002. Comparative physiology of salt and water stress. Plant Cell Environ. 25, 239–250. https://doi.org/10.1046/j.0016-8025.2001.00808.x

Munns, R., Day, D.A., Fricke, W., Watt, M., Arsova, B., Barkla, B.J., Bose, J., Byrt, C.S., Chen, Z.-H., Foster, K.J., Gilliham, M., Henderson, S.W., Jenkins, C.L.D., Kronzucker, H.J., Miklavcic, S.J., Plett, D., Roy, S.J., Shabala, S., Shelden, M.C., Soole, K.L., Taylor, N.L., Tester, M., Wege, S., Wegner, L.H., Tyerman, S.D., 2020a. Energy costs of salt tolerance in crop plants. New Phytol. 225, 1072–1090. https://doi.org/10.1111/nph.15864

Munns, R., Passioura, J.B., Colmer, T.D., Byrt, C.S., 2020b. Osmotic adjustment and energy limitations to plant growth in saline soil. New Phytol. 225, 1091–1096. https://doi.org/10.1111/nph.15862

Munns, R., Tester, M., 2008. Mechanisms of salinity tolerance. Annu. Rev. Plant Biol. 59, 651–681. https://doi.org/10.1146/annurev.arplant.59.032607.092911

Nakabayashi, R., Yonekura-Sakakibara, K., Urano, K., Suzuki, M., Yamada, Y., Nishizawa, T., Matsuda, F., Kojima, M., Sakakibara, H., Shinozaki, K., Michael, A.J., Tohge, T., Yamazaki, M., Saito, K., 2014. Enhancement of oxidative and drought tolerance in *Arabidopsis* by overaccumulation of antioxidant flavonoids. Plant J. 77, 367–379. https://doi.org/10.1111/tpj.12388

Neess, D., Bek, S., Engelsby, H., Gallego, S.F., Færgeman, N.J., 2015. Long-chain acyl-CoA esters in metabolism and signaling: Role of acyl-CoA binding proteins. Prog. Lipid Res. 59, 1–25. https://doi.org/10.1016/j.plipres.2015.04.001

Neves, G.Y.S., Marchiosi, R., Ferrarese, M.L.L., Siqueira-Soares, R.C., Ferrarese-Filho, O., 2010. Root growth inhibition and lignification induced by salt stress in soybean. J. Agron. Crop Sci. 196, 467–473. https://doi.org/10.1111/j.1439-037X.2010.00432.x

Nguyen, H.T., Meir, P., Sack, L., Evans, J.R., Oliveira, R.S., Ball, M.C., 2017. Leaf water storage increases with salinity and aridity in the mangrove *Avicennia marina*: Integration of leaf structure, osmotic adjustment and access to multiple water sources. Plant Cell Environ. 40, 1576–1591. https://doi.org/10.1111/pce.12962

Nothias, L.-F., Petras, D., Schmid, R., Dührkop, K., Rainer, J., Sarvepalli, A., Protsyuk, I., Ernst, M., Tsugawa, H., Fleischauer, M., Aicheler, F., Aksenov, A.A., Alka, O., Allard, P.-M., Barsch, A., Cachet, X., Caraballo-Rodriguez, A.M., Da Silva, R.R., Dang, T., Garg, N., Gauglitz, J.M., Gurevich, A., Isaac, G., Jarmusch, A.K., Kameník, Z., Kang, K.B., Kessler, N., Koester, I., Korf, A., Le Gouellec, A., Ludwig, M., Martin H., C., McCall, L.-I., McSayles, J., Meyer, S.W., Mohimani, H., Morsy, M., Moyne, O., Neumann, S., Neuweger, H., Nguyen, N.H., Nothias-Esposito, M., Paolini, J., Phelan, V.V., Pluskal, T., Quinn, R.A., Rogers, S., Shrestha, B., Tripathi, A., van der Hooft, J.J.J., Vargas, F., Weldon, K.C., Witting, M., Yang, H., Zhang, Z., Zubeil, F., Kohlbacher, O., Böcker, S., Alexandrov, T., Bandeira, N., Wang, M., Dorrestein, P.C., 2020. Feature-based molecular networking in the GNPS analysis environment. Nat. Methods 17, 905–908. https://doi.org/10.1038/s41592-020-0933-6

Osawa, H., Endo, I., Hara, Y., Matsushima, Y., Tange, T., 2011. Transient proliferation of proanthocyanidin-accumulating cells on the epidermal apex contributes to highly aluminum-resistant root elongation in camphor tree. Plant Physiol. 155, 433–446. https://doi.org/10.1104/pp.110.166967

Ottow, E.A., Brinker, M., Teichmann, T., Fritz, E., Kaiser, W., Brosché, M., Kangasjärvi, J., Jiang, X., Polle, A., 2005. *Populus euphratica* displays apoplastic sodium accumulation, osmotic adjustment by decreases in calcium and soluble carbohydrates, and develops leaf succulence under salt stress. Plant Physiol. 139, 1762–1772. https://doi.org/10.1104/pp.105.069971

Pichersky, E., Raguso, R.A., 2018. Why do plants produce so many terpenoid compounds? New Phytol. 220, 692–702. https://doi.org/10.1111/nph.14178

Pobłocka-Olech, L., van Nederkassel, A.-M., Vander Heyden, Y., Krauze-Baranowska, M., Glód, D., Baczek, T., 2007. Chromatographic analysis of salicylic compounds in different species of the genus *Salix*. J. Sep. Sci. 30, 2958–2966. https://doi.org/10.1002/jssc.200700137

Prasad, R., Shivay, Y.S., 2018. Sulphur in soil, plant and human nutrition. Proc. Natl. Acad. Sci. India Sect. B Biol. Sci. 88, 429–434. https://doi.org/10.1007/s40011-016-0769-0

Quinn, L.D., Straker, K.C., Guo, J., Kim, S., Thapa, S., Kling, G., Lee, D.K., Voigt, T.B., 2015. Stress-tolerant feedstocks for sustainable bioenergy production on marginal land. BioEnergy Res. 8, 1081–1100. https://doi.org/10.1007/s12155-014-9557-y

R Core Team, 2022. R: A Language and environment for statistical computing.

Rausch, T., Wachter, A., 2005. Sulfur metabolism: a versatile platform for launching defence operations. Trends Plant Sci. 10, 503–509. https://doi.org/10.1016/j.tplants.2005.08.006

Reginato, M., Luna, V., Papenbrock, J., 2021. Current knowledge about Na2SO4 effects on plants: What is different in comparison to NaCl? J. Plant Res. 134, 1159–1179. https://doi.org/10.1007/s10265-021-01335-y

Reich, M., Aghajanzadeh, T., Helm, J., Parmar, S., Hawkesford, M.J., De Kok, L.J., 2017. Chloride and sulfate salinity differently affect biomass, mineral nutrient composition and expression of sulfate transport and assimilation genes in *Brassica rapa*. Plant Soil 411, 319–332. https://doi.org/10.1007/s11104-016-3026-7

Reyt, G., Ramakrishna, P., Salas-González, I., Fujita, S., Love, A., Tiemessen, D., Lapierre, C., Morreel, K., Calvo-Polanco, M., Flis, P., Geldner, N., Boursiac, Y., Boerjan, W., George, M.W., Castrillo, G., Salt, D.E., 2021. Two chemically distinct root lignin barriers control solute and water balance. Nat. Commun. 12, 2320. https://doi.org/10.1038/s41467-021-22550-0

Richter, J.A., Behr, J.H., Erban, A., Kopka, J., Zörb, C., 2019. Ion-dependent metabolic responses of *Vicia faba* L. to salt stress. Plant Cell Environ. 42, 295–309. https://doi.org/10.1111/pce.13386

Rodriguez, H.G., Roberts, JKM., Jordan, W.R., Drew, M.C., 1997. Growth, water relations, and accumulation of organic and inorganic solutes in roots of maize seedlings during salt stress. Plant Physiol. 113, 881–893. https://doi.org/10.1104/pp.113.3.881

Rodzkin, A., Volk, T., 2018. Using schrub willow for biological reclamation of areas with raised soil salinity. Presented at the 12th Eco-conference® on environmental protection of urban and suburban settlements, Novi Sad, Serbia.

Rohart, F., Gautier, B., Singh, A., Cao, K.-A.L., 2017. mixOmics: An R package for 'omics feature selection and multiple data integration. PLOS Comput. Biol. 13, e1005752. https://doi.org/10.1371/journal.pcbi.1005752

Ryu, H., Cho, Y.-G., 2015. Plant hormones in salt stress tolerance. J. Plant Biol. 58, 147–155. https://doi.org/10.1007/s12374-015-0103-z

Sanchez, D.H., Siahpoosh, M.R., Roessner, U., Udvardi, M., Kopka, J., 2008. Plant metabolomics reveals conserved and divergent metabolic responses to salinity. Physiol. Plant. 132, 209–219. https://doi.org/10.1111/j.1399-3054.2007.00993.x

Sas, E., Hennequin, L.M., Frémont, A., Jerbi, A., Legault, N., Lamontagne, J., Fagoaga, N., Sarrazin, M., Hallett, J.P., Fennell, P.S., Barnabé, S., Labrecque, M., Brereton, N.J.B., Pitre, F.E., 2021. Biorefinery potential of sustainable municipal wastewater treatment using fast-growing willow. Sci. Total Environ. 792, 148146. https://doi.org/10.1016/j.scitotenv.2021.148146

Sasse, J., Martinoia, E., Northen, T., 2018. Feed your friends: Do plant exudates shape the root microbiome? Trends Plant Sci. 23, 25–41. https://doi.org/10.1016/j.tplants.2017.09.003

Schmid, R., Heuckeroth, S., Korf, A., Smirnov, A., Myers, O., Dyrlund, T.S., Bushuiev, R., Murray, K.J., Hoffmann, N., Lu, M., Sarvepalli, A., Zhang, Z., Fleischauer, M., Dührkop, K., Wesner, M., Hoogstra, S.J., Rudt, E., Mokshyna, O., Brungs, C., Ponomarov, K., Mutabdžija, L., Damiani, T., Pudney, C.J., Earll, M., Helmer, P.O., Fallon, T.R., Schulze, T., Rivas-Ubach, A., Bilbao, A., Richter, H., Nothias, L.-F., Wang, M., Orešič, M., Weng, J.-K., Böcker, S., Jeibmann, A., Hayen, H., Karst, U., Dorrestein, P.C., Petras, D., Du, X., Pluskal, T., 2023. Integrative analysis of multimodal mass spectrometry data in MZmine 3. Nat. Biotechnol. 41, 447–449. https://doi.org/10.1038/s41587-023-01690-2

Schymanski, E.L., Jeon, J., Gulde, R., Fenner, K., Ruff, M., Singer, H.P., Hollender, J., 2014. Identifying small molecules via high resolution mass spectrometry: Communicating confidence. Environ. Sci. Technol. 48, 2097–2098. https://doi.org/10.1021/es5002105

Shannon, P., Markiel, A., Ozier, O., Baliga, N.S., Wang, J.T., Ramage, D., Amin, N., Schwikowski, B., Ideker, T., 2003. Cytoscape: A software environment for integrated models of biomolecular interaction networks. Genome Res. 13, 2498–2504. https://doi.org/10.1101/gr.1239303

Shavrukov, Y., 2013. Salt stress or salt shock: Which genes are we studying? J. Exp. Bot. 64, 119–127. https://doi.org/10.1093/jxb/ers316

Si, C.-L., Kim, J.-K., Bae, Y.-S., Li, S.-M., 2009. Phenolic compounds in the leaves of *Populus ussuriensis* and their antioxidant activities. Planta Med. 75, 1165–1167. https://doi.org/10.1055/s-0029-1185476

Singh, A., 2021. Soil salinization management for sustainable development: A review. J. Environ. Manage. 277, 111383. https://doi.org/10.1016/j.jenvman.2020.111383

Skerrett, M., Tyerman, S.D., 1994. A channel that allows inwardly directed fluxes of anions in protoplasts derived from wheat roots. Planta 192, 295–305. https://doi.org/10.1007/BF00198563

Slama, I., Abdelly, C., Bouchereau, A., Flowers, T., Savouré, A., 2015. Diversity, distribution and roles of osmoprotective compounds accumulated in halophytes under abiotic stress. Ann. Bot. 115, 433–447. https://doi.org/10.1093/aob/mcu239

Sonar, P., Bellucci, L., Mossa, A., Heidarsson, P.O., Kragelund, B.B., Cecconi, C., 2020. Effects of ligand binding on the energy landscape of acyl-CoA-binding protein. Biophys. J. 119, 1821–1832. https://doi.org/10.1016/j.bpj.2020.09.016

Sonmez, S., Buyuktas, D., Okturen, F., Citak, S., 2008. Assessment of different soil to water ratios (1:1, 1:2.5, 1:5) in soil salinity studies. Geoderma, Antarctic Soils and Soil Forming Processes in a Changing Environment 144, 361–369. https://doi.org/10.1016/j.geoderma.2007.12.005

Sui, D., Wang, B., 2020. Transcriptome analysis reveals complex defensive mechanisms in salt-tolerant and salt-sensitive shrub willow genotypes under salinity stress. Int. J. Genomics 2020, e6870157. https://doi.org/10.1155/2020/6870157

Sumner, L.W., Amberg, A., Barrett, D., Beale, M.H., Beger, R., Daykin, C.A., Fan, T.W.-M., Fiehn, O., Goodacre, R., Griffin, J.L., Hankemeier, T., Hardy, N., Harnly, J., Higashi, R., Kopka, J., Lane, A.N., Lindon, J.C., Marriott, P., Nicholls, A.W., Reily, M.D., Thaden, J.J., Viant, M.R., 2007. Proposed minimum reporting standards for chemical analysis. Metabolomics 3, 211–221. https://doi.org/10.1007/s11306-007-0082-2

Teakle, N.L., Tyerman, S.D., 2010. Mechanisms of Cl- transport contributing to salt tolerance. Plant Cell Environ. 33, 566–589. https://doi.org/10.1111/j.1365-3040.2009.02060.x

Tyśkiewicz, K., Konkol, M., Kowalski, R., Rój, E., Warmiński, K., Krzyżaniak, M., Gil, Ł., Stolarski, M.J., 2019. Characterization of bioactive compounds in the biomass of black locust, poplar and willow. Trees 33, 1235–1263. https://doi.org/10.1007/s00468-019-01837-2

van Zelm, E., Zhang, Y., Testerink, C., 2020. Salt tolerance mechanisms of plants. Annu. Rev. Plant Biol. 71, 403–433. https://doi.org/10.1146/annurev-arplant-050718-100005

Volf, M., Hrcek, J., Julkunen-Tiitto, R., Novotny, V., 2015. To each its own: differential response of specialist and generalist herbivores to plant defence in willows. J. Anim. Ecol. 84, 1123–1132. https://doi.org/10.1111/1365-2656.12349

Volk, T.A., Abrahamson, L.P., Nowak, C.A., Smart, L.B., Tharakan, P.J., White, E.H., 2006. The development of short-rotation willow in the northeastern United States for bioenergy and bioproducts, agroforestry and phytoremediation. Biomass Bioenergy, Proceedings of the 5th Biennial meeting of the Short Rotation Woody Crops Operations Working Group in conjunction with International Energy Agency Bioenergy, Task 30, Short Rotation Crops for Bioenergy Systems and International Union of Forest Research Organization, Working Unit 1.09.01, Integrated Research in Temperate Short-Rotation Energy Plantations 30, 715–727. https://doi.org/10.1016/j.biombioe.2006.03.001

Watanabe, M., Hoefgen, R., 2019. Sulphur systems biology: Making sense of omics data. J. Exp. Bot. 70, 4155–4170. https://doi.org/10.1093/jxb/erz260

Watanabe, S., Kojima, K., Ide, Y., Sasaki, S., 2000. Effects of saline and osmotic stress on proline and sugar accumulation in *Populus euphratica in vitro*. Plant Cell Tissue Organ Cult. 63, 199–206. https://doi.org/10.1023/A:1010619503680

Wege, S., Gilliham, M., Henderson, S.W., 2017. Chloride: not simply a 'cheap osmoticum', but a beneficial plant macronutrient. J. Exp. Bot. 68, 3057–3069. https://doi.org/10.1093/jxb/erx050

973 Wei, H., Movahedi, A., Xu, C., Sun, W., Li, L., Wang, P., Li, D., Zhuge, Q., 2020. Overexpression of PtHMGR
974 enhances drought and salt tolerance of poplar. Ann. Bot. 125, 785–803.
975 https://doi.org/10.1093/aob/mcz158
976 White, P.J., Broadley, M.R., 2001. Chloride in soils and its uptake and movement within the plant: A review.
977 Ann. Bot. 88, 967–988. https://doi.org/10.1006/anbo.2001.1540
978 Wu, D., Cai, S., Chen, M., Ye, L., Chen, Z., Zhang, H., Dai, F., Wu, F., Zhang, G., 2013. Tissue metabolic responses
979 to salt stress in wild and cultivated barley. PLOS ONE 8, e55431.
980 https://doi.org/10.1371/journal.pone.0055431
981 Xia, L., Xiaodong, M., Yunhe, C., Junxiang, L., Junzhu, Z., Feifei, Z., Zhenyuan, S., Lei, H., 2021. Transcriptomic
982 and metabolomic insights into the adaptive response of *Salix viminalis* to phenanthrene. Chemosphere
983 262, 127573. https://doi.org/10.1016/j.chemosphere.2020.127573
984 Xiao, J., Muzashvili, T.S., Georgiev, M.I., 2014. Advances in the biotechnological glycosylation of valuable
985 flavonoids. Biotechnol. Adv. 32, 1145–1156. https://doi.org/10.1016/j.biotechadv.2014.04.006
986 Yancey, P.H., 2005. Organic osmolytes as compatible, metabolic and counteracting cytoprotectants in high
987 osmolarity and other stresses. J. Exp. Biol. 208, 2819–2830. https://doi.org/10.1242/jeb.01730
988 Yang, Y., Guo, Y., 2018. Elucidating the molecular mechanisms mediating plant salt-stress responses. New
989 Phytol. 217, 523–539. https://doi.org/10.1111/nph.14920
990 Zhang, Y., Fang, J., Wu, X., Dong, L., 2018. Na+/K+ balance and transport regulatory mechanisms in weedy and
991 cultivated rice (Oryza sativa L.) under salt stress. BMC Plant Biol. 18, 375.
992 https://doi.org/10.1186/s12870-018-1586-9
993 Zhou, J., Guo, J., Chen, Q., Wang, B., He, X., Zhuge, Q., Wang, P., 2022. Different color regulation mechanism in
994 willow barks determined using integrated metabolomics and transcriptomics analyses. BMC Plant Biol.
995 22, 530. https://doi.org/10.1186/s12870-022-03909-x
996 Zhou, J., Huang, J., Tian, X., Zheng, J., He, X., 2020. Transcriptome analysis reveals dynamic changes in the salt
997 stress response in *Salix*. J. For. Res. 31, 1851–1862. https://doi.org/10.1007/s11676-019-00941-w
998 Zhou, Z., Luo, M., Zhang, H., Yin, Y., Cai, Y., Zhu, Z.-J., 2022. Metabolite annotation from knowns to unknowns
999 through knowledge-guided multi-layer metabolic networking. Nat. Commun. 13, 6656.
1000 https://doi.org/10.1038/s41467-022-34537-6
1001 Zörb, C., Geilfus, C.-M., Dietz, K.-J., 2019. Salinity and crop yield. Plant Biol. 21, 31–38.
1002 https://doi.org/10.1111/plb.12884
1003 Zou, Y., Zhang, Y., Testerink, C., 2022. Root dynamic growth strategies in response to salinity. Plant Cell Environ.
1004 45, 695–704. https://doi.org/10.1111/pce.14205
1005

1006 **11 MAIN FIGURES**

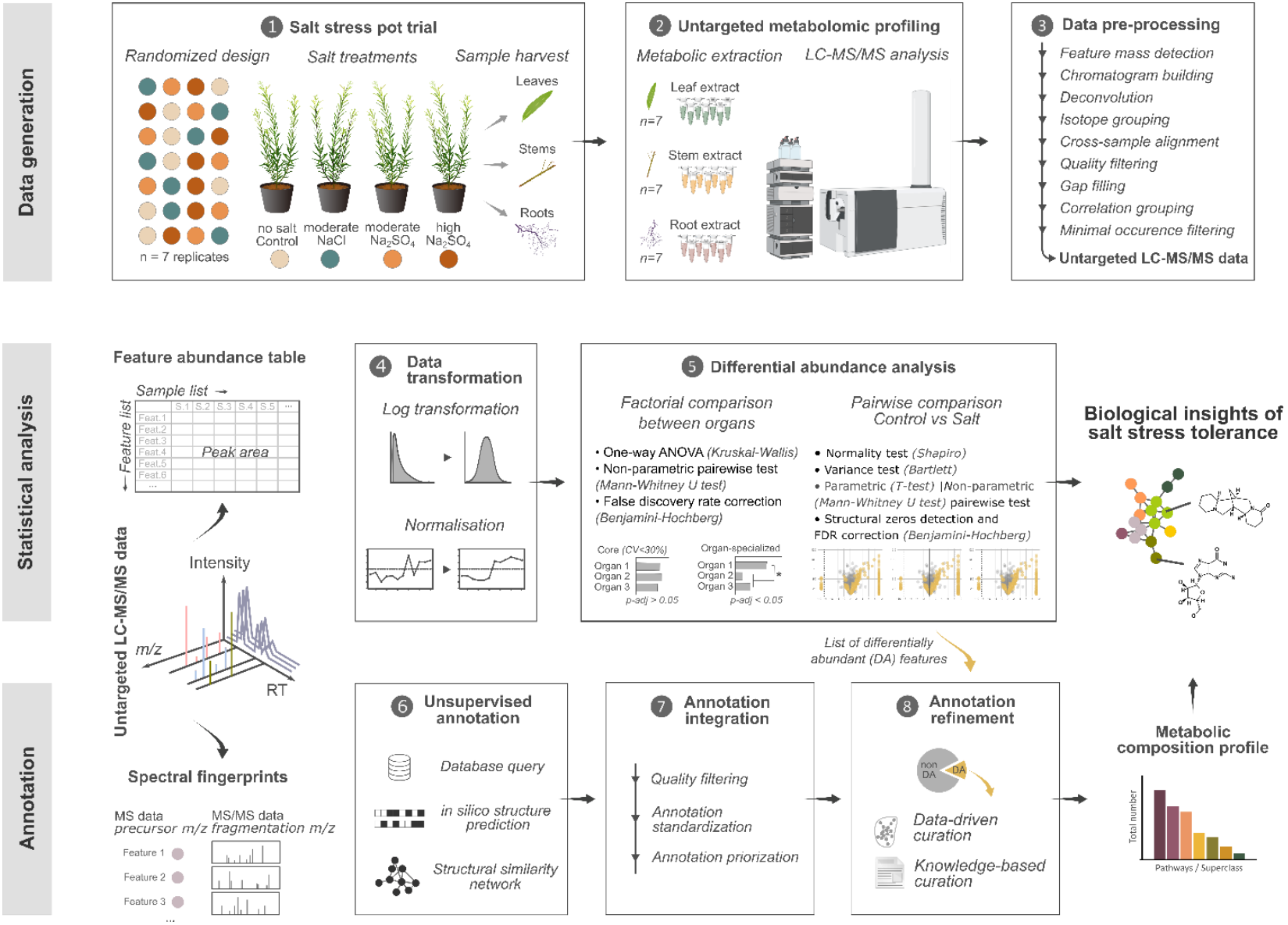

***Figure 1**: Workflow for untargeted metabolomics approach.*

A randomized pot trial treated willows with salt solutions or water controls (7 replicates per treatment) to explore variation in anion-specific salt tolerance mechanisms across organs. Metabolites were extracted from root, stem and leaf samples and analysed by LC-MS/MS. Resulting chromatographic data were pre-processed using MZmine for features mass detection, cross-sample alignment and quality filters. Statistical analysis used a cross-sample aligned peak area table. After log transformation and Eigen MS normalization, univariate analysis was used to factorially compare feature peak areas across willow organs in controls, while pairwise comparisons were used to identify differentially abundant (DA) compounds between each salt treatment compared to controls. Parametric or non-parametric tests were used based on feature peak area normality and variance homogeneity before a false discovery rate correction was applied to account for multiple testing. Annotation strategy used precursors information and corresponding spectral fingerprints (when available) to query multiple databases and for *in silico* structure prediction to generate a list of annotation candidates (unsupervised annotation). After standardizing compounds identity information and assigning prioritization criteria, the best candidate was retained. Annotation was further refined for compounds identified as differentially abundant due to salt treatment and used data-driven (structural similarity networking) and knowledge-driven (literature) curation.

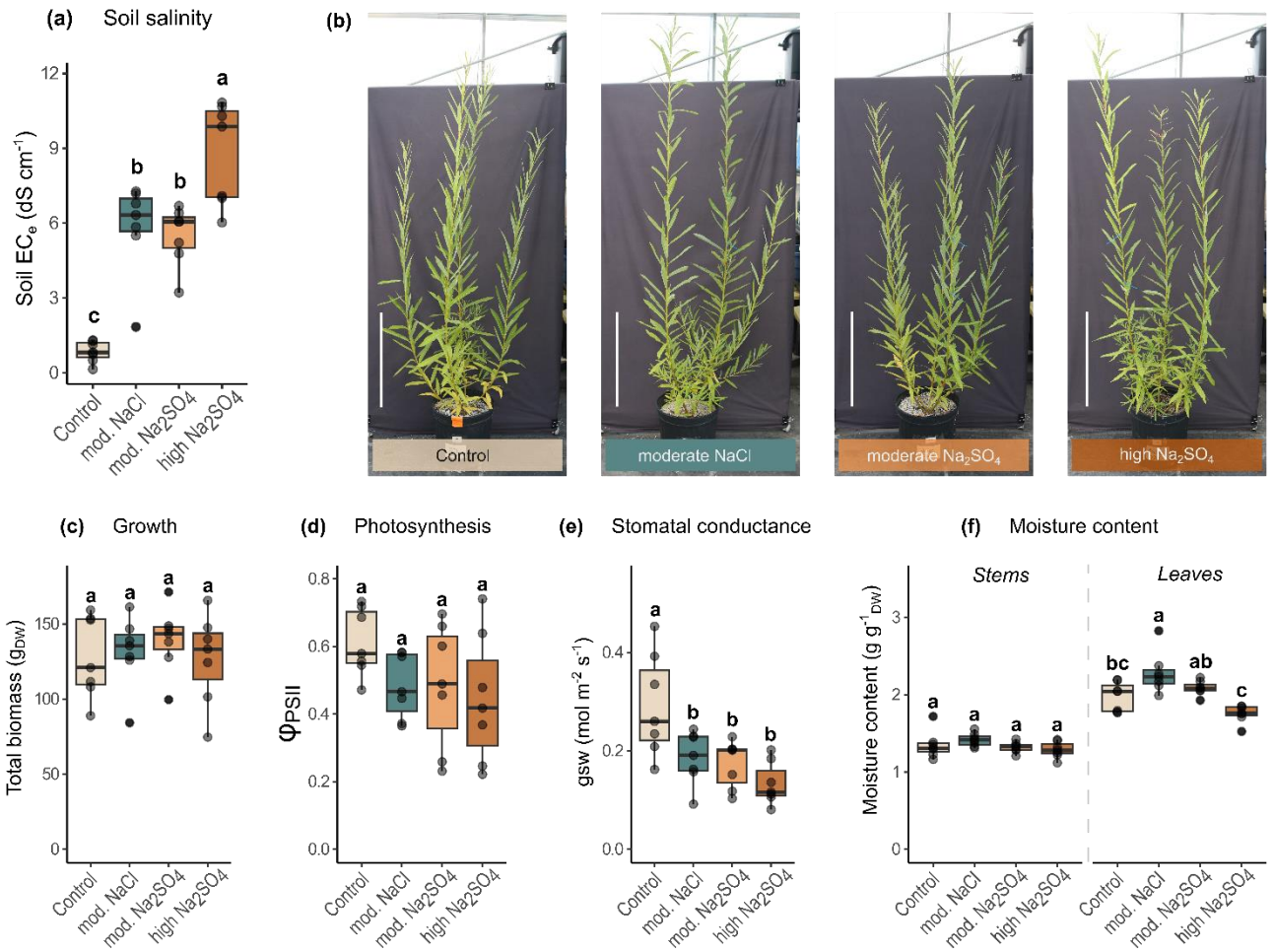

Figure 2: Physiological assessment of salt stress on Salix miyabeana 'SX64'.

(a) Following 56 days of root establishment, salinity in planted pots was progressively built-up over 28 days to reach the final saturated soil electroconductivity (EC), as inferred from a (1:1) soil-to-water extract. **(b)** Representative willow photographs, on harvest day, in response to salt treatments (white scale bars: 50 cm). The impact of moderate NaCl, moderate Na_2SO_4 and high Na_2SO_4 were quantified on **(c)** total biomass (dry weight), **(d)** photosystem II efficiency evaluated using the LI-COR 600 parameter phiPSII, **(e)** stomatal conductance gsw, **(f)** stems and leaves moisture contents. Boxes represent median and quartiles while whiskers extend to the largest value within 1.5 times the inter-quartile range (IQR) from the hinge. Dots represent individual plants (n=7). Significant differences ($p<0.05$) indicated by letters were determined by two-way ANOVA followed by Tukey's post hoc test.

1018

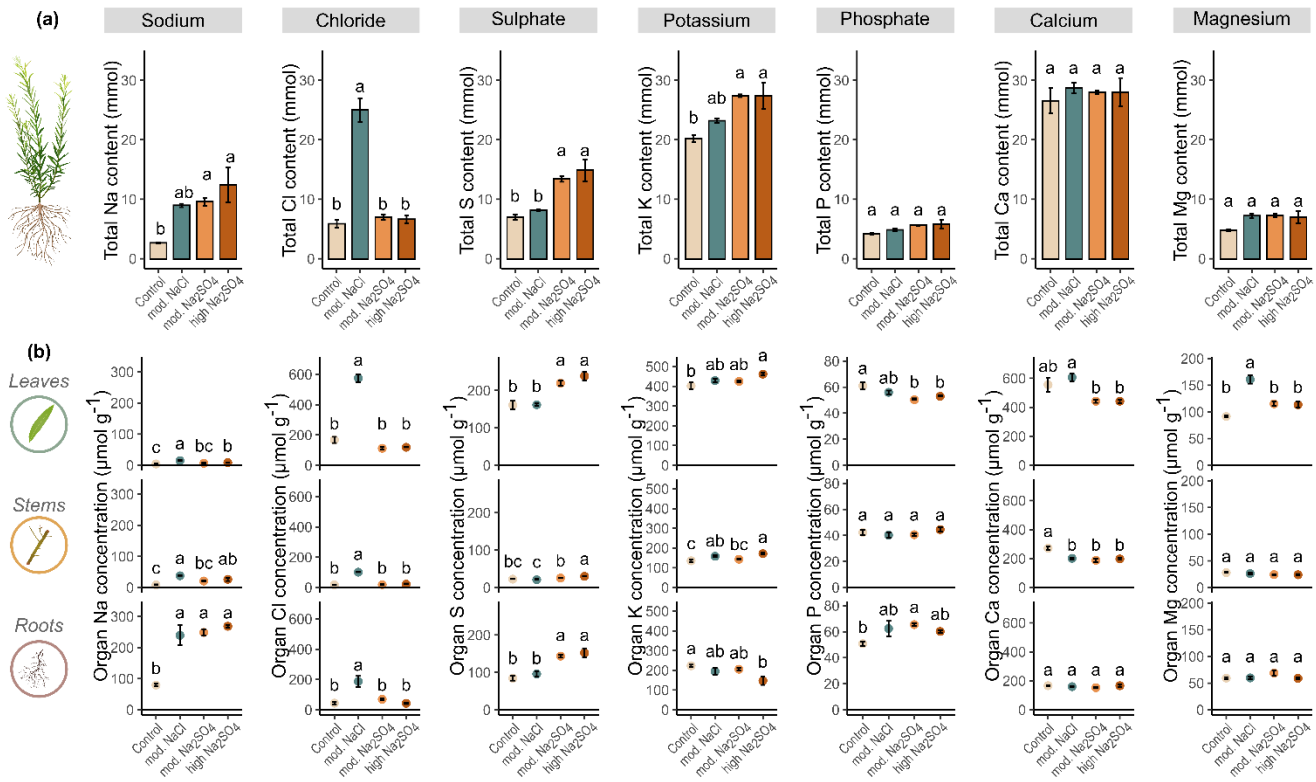

Figure 3: Elemental analysis of mineral nutrients.

Elemental analyses include sodium (Na), chloride (Cl), sulphur (S), potassium (K), phosphorus (P), calcium (Ca), and magnesium (Mg). **(a)** Total element content (mmol) combined from the leaves, stems and roots presented. The bars indicate mean values within each organ ± standard error (n=3). **(b)** Element concentration within a single organ (µmol g_{DW}^{-1}) is shown. The dots represent mean values ± standard error (n=3). Letters indicate significant differences ($p<0.05$) between control, moderate NaCl, moderate Na_2SO_4, and high Na_2SO_4 treatments and were determined using two-way ANOVA followed by Tukey's post hoc test. Mineral elements ratios (K^+/Na^+; Ca^{2+}/Na^+; K^+/Ca^{2+}) are presented in Supporting information – Fig.S4.

1019

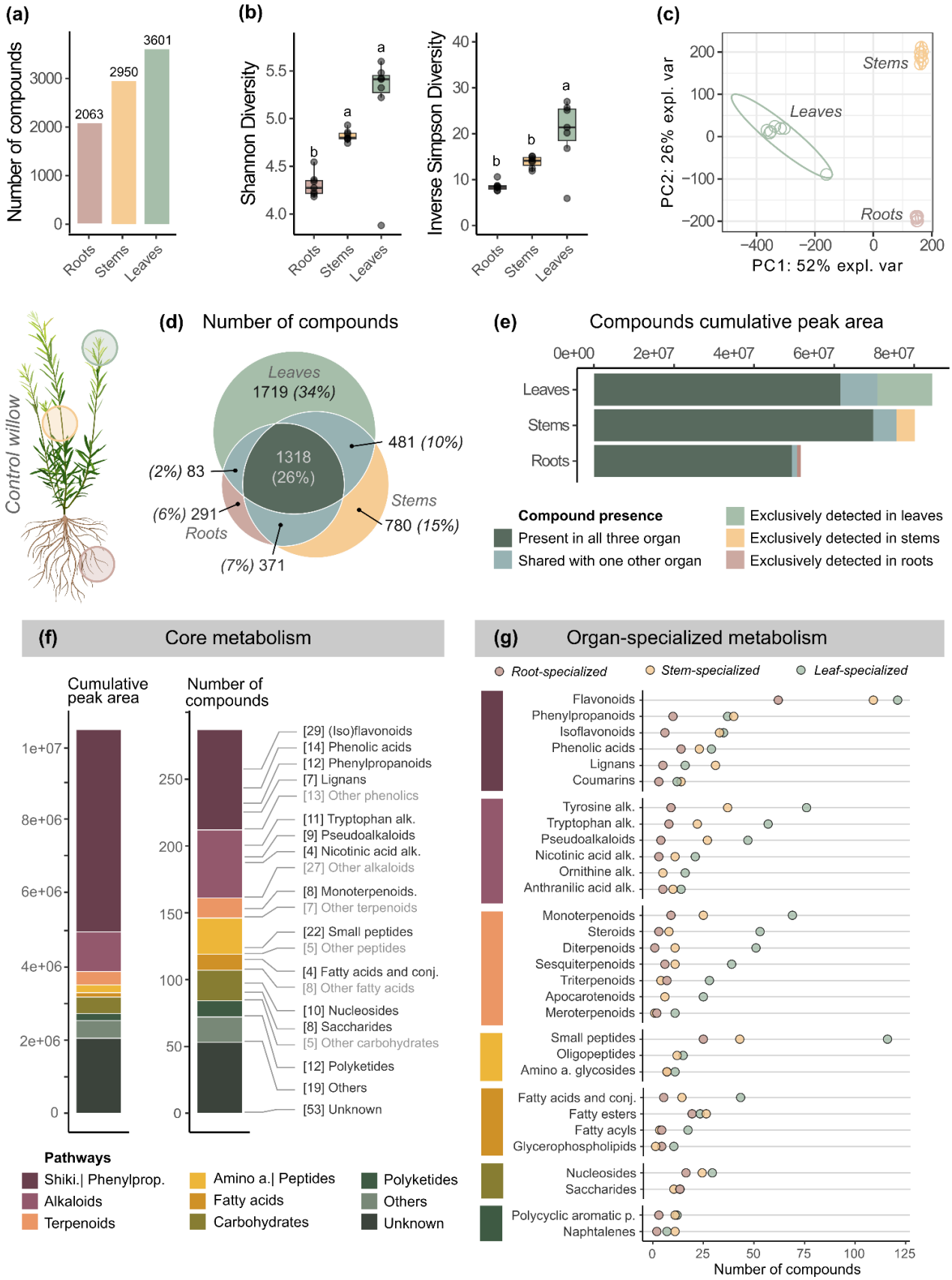

Figure 4: Willow metabolic composition.

Organs (leaves, stems and roots) were separately collected from control willows and analysed for metabolomic profiling. **(a)** Total number of consistently detected metabolites within each major organ (present in at least 4

replicates out of 7). **(b)** Comparison of organ metabolic richness using Shannon and Inverse Simpson diversity indices (n=7), different letters indicate significant differences (ANOVA, Tukey HSD, $p<0.05$). **(c)** Principal component analysis depicting dissimilarity in organ composition based on Bray-Curtis distances, ellipses are for standard deviation. **(d)** Venn diagram illustrating the distribution of metabolites across organs as unique to one or shared between multiple. **(e)** Cumulative peak areas of metabolites present in each organ, categorised based on their exclusive presence in the respective organ or shared across multiple organs. **(f)** Cumulative peak area and number of core metabolites (compounds present across the entire plant, with no significant variation of abundance between organs) classified per metabolic pathways, with composition details of main superclasses. **(g)** Count of compounds significantly higher in one organ compared to the other two (ANOVA, Tukey HSD, $p<0.05$), revealing dominant organ-specialisation of some metabolic superclasses.

1020

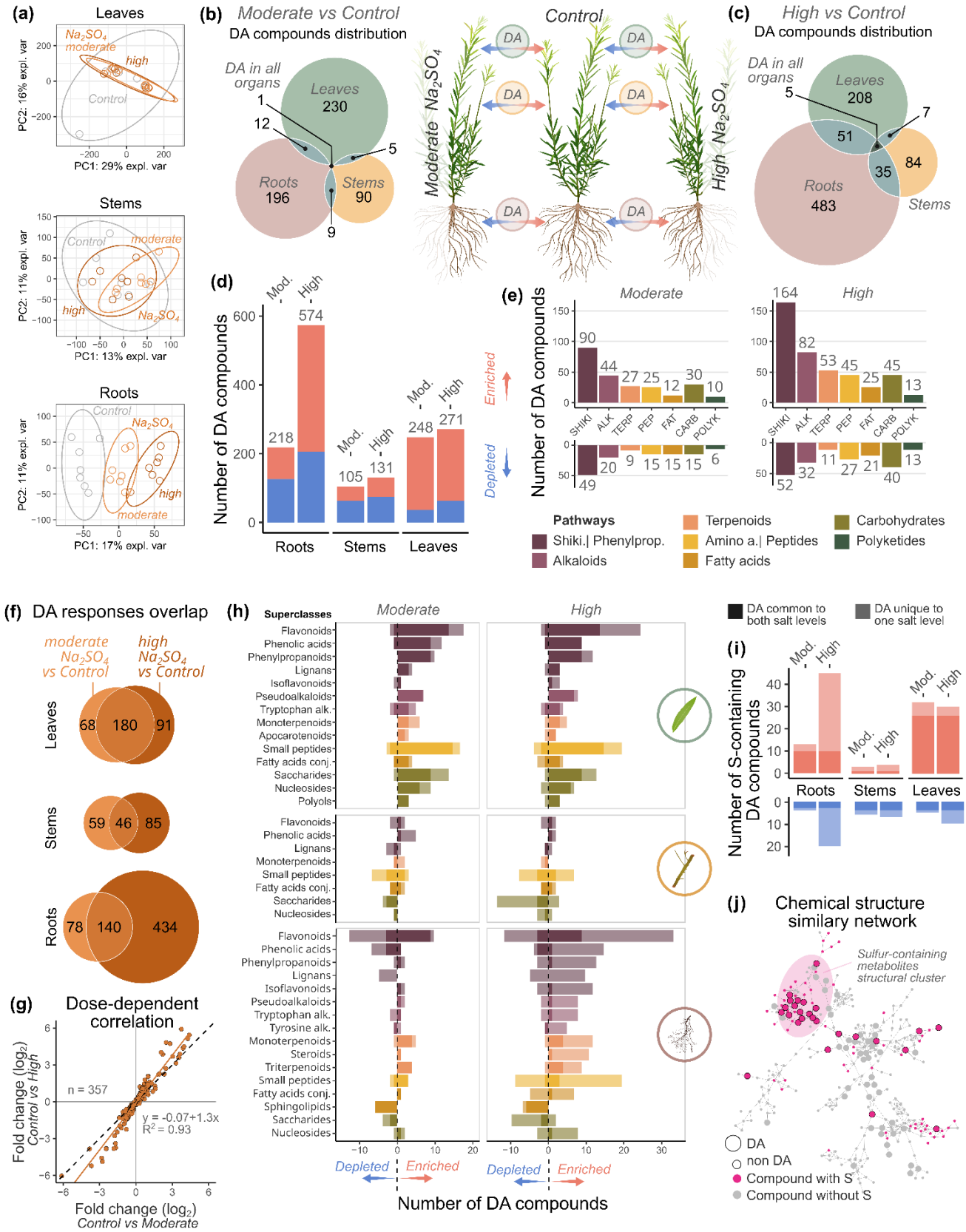

Figure 5: Willow metabolic response to sodium sulphate (Na_2SO_4) salt and its variation with dose

(a) Principal component analysis (PCA) based on Bray-Curtis distance, illustrating metabolic profile dissimilarity between control, moderate Na_2SO_4 and high Na_2SO_4 at organ scale (n=7), including standard deviation ellipse

(95% confidence interval). **(b)** Organ distribution of differentially abundant (DA) compounds between control and moderate concentration Na_2SO_4-treated willows ($p<0.05$). **(c)** Organ distribution of differentially abundant compounds between control and high concentration Na_2SO_4-treated willows ($p<0.05$). **(d)** Overview of significantly enriched and depleted compounds across organs, comparing DA of control against moderate Na_2SO_4 and control against high Na_2SO_4. **(e)** Distribution of enriched and depleted DA compounds across metabolic pathways for moderate and high Na_2SO_4 treatments compared to controls. **(f)** Metabolic response overlap across both Na_2SO_4 concentrations, representing the number of DA compounds common and unique to a single dose DA, at organ scale. **(g)** Dose-dependent correlation of compounds consistently DA across Na_2SO_4 levels within the same organ (excluding salt-induced/salt-suppressed compounds with infinite fold change), representing the fold change (log2) of average peak areas (n=7) under moderate Na_2SO_4 relative to control against high Na_2SO_4 relative to control. **(h)** Sub-selection of main superclasses altered by moderate or high concentration of Na_2SO_4 compared to controls, illustrating enriched and depleted compounds distribution at organ scale. DA compounds shared between both treatment levels are highlighted by the darker section of the bars. **(i)** Distribution of enriched and depleted sulphur-containing DA compounds at organ scale, comparing both levels of Na_2SO_4. Shared compounds are highlighted by the darker section of the bars. **(j)** Molecular network of compounds MS/MS spectra similarities (cosine >0.6) computed in the GNPS environment and visualised in Cytoscape. Dots are color-coded based on the presence of sulphur (pink represents S-containing compounds) and dot size highlights significantly different compounds (larger dots are DA compounds). A major cluster containing 16 S-containing and structurally similar DA compounds is circled by an ellipse.

1021

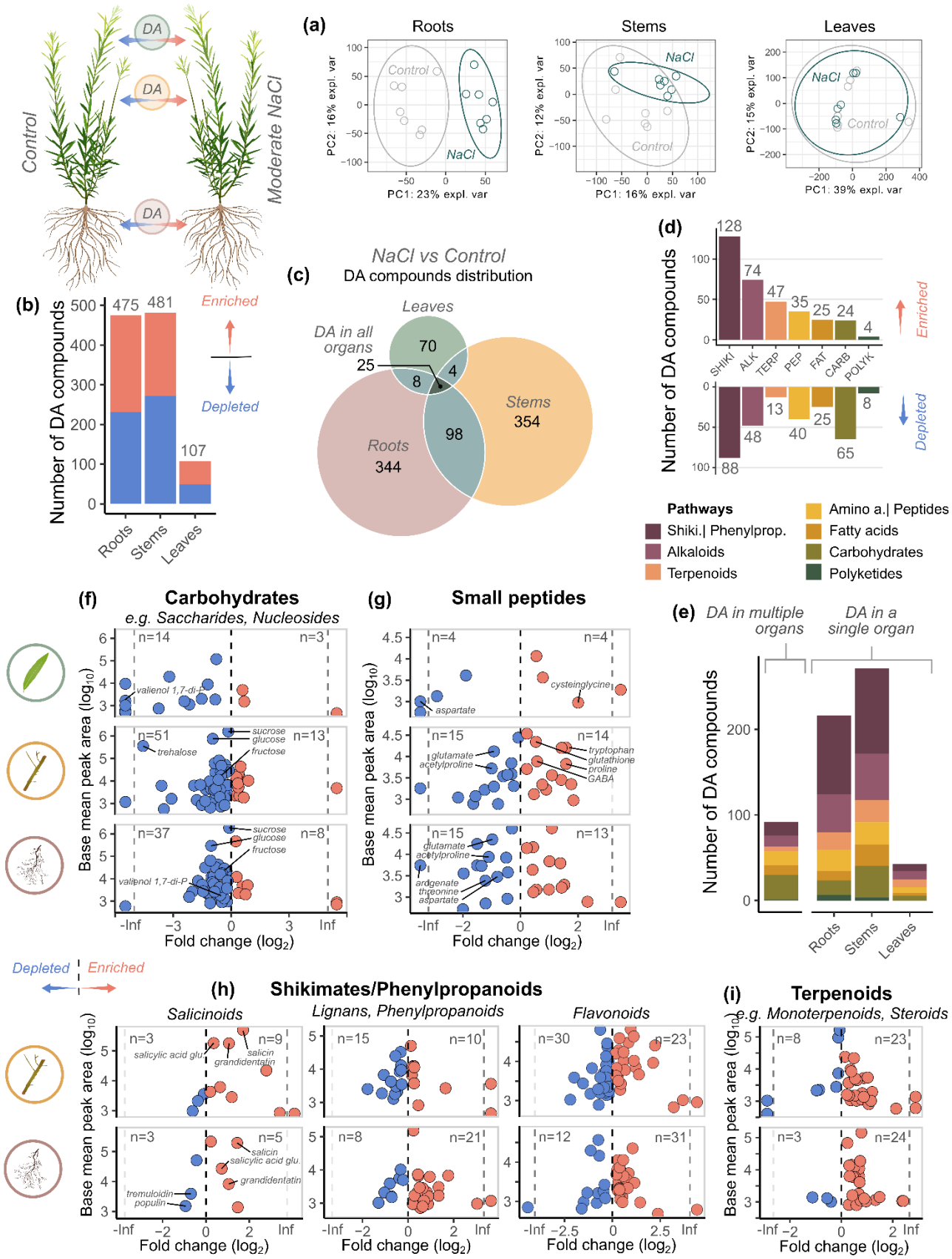

Figure 6: Willow metabolic response to sodium chloride (NaCl) salt.

(a) Principal component analysis (PCA) based on Bray-Curtis distance, illustrating metabolic profile dissimilarity between control and moderate NaCl at organ scale (n=7), including standard deviation ellipse (95% confidence

interval) **(b)** Overview of significantly enriched and depleted compounds across organs. **(c)** Organ distribution of differentially abundant (DA) compounds between control and moderate concentration NaCl-treated willows ($p<0.05$). **(d)** Distribution of enriched and depleted DA compounds across metabolic pathways. **(e)** Metabolic profile at pathway level of DA compounds shared between multiple organs and unique to roots, stems or leaves. Sub-selection of main pathways or superclasses altered by moderate NaCl compared to controls, illustrating enriched and depleted compounds distribution at organ scale for **(f)** carbohydrates, including saccharides and nucleosides, **(g)** small peptides, **(h)** and 3 major superclass of shikimates and phenylpropanoids pathway: salicinoids, lignans, phenylpropanoids, flavonoids, as well as **(i)** terpenoids, including monoterpenoids and steroids. Dots are color-coded by regulation (blue: depleted, red: enriched by salt treatment compared to control). Base mean area reflects average peak area across all compared samples.

1022

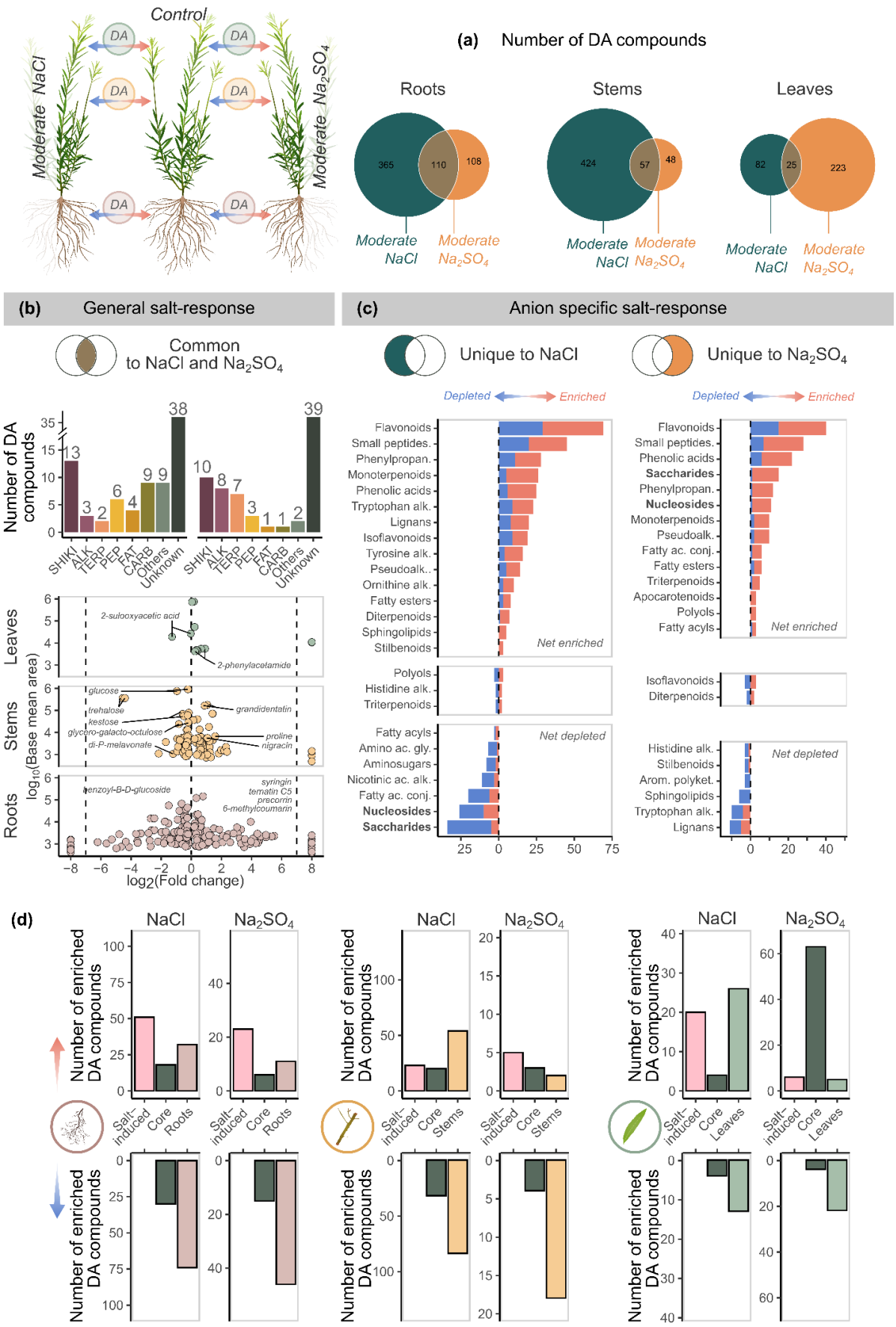

Figure 7: General willow salt response and anion specific tailored responses.

(a) Venn diagrams showing DA metabolic responses overlap in roots, stems, and leaves under moderate NaCl and Na_2SO_4 stress. **(b**) Pathway profile of commonly enriched and depleted compounds in response to moderate salt stress. Fold change graph illustrated enriched and depleted compounds distribution at organ scale. **(c)** Superclass profiles of NaCl- and Na_2SO_4-specific responses. Superclasses are categorized as net enriched, equal, or net depleted based on the relative number of enriched versus depleted compounds. Differential patterns for nucleosides and saccharides are highlighted in bold. **(d)** Metabolic response to moderate NaCl and moderate Na_2SO_4 categorised based on compounds distribution across the whole plant: salt-induced compounds (not detected in controls), core compounds (present in all organs at stable state in controls), organ-specialised compounds: roots, stems or leaves (present in a higher abundance in a specific organ, based on controls). Bar graphs are split as depleted and enriched compounds to highlight patterning of the DA compounds.

1025